

NASA TECHNICAL NOTE



NASA TN D-6265

2,1

LOAN COPY: RET
AFWL (DOG
KIRTLAND AFB

0133072



NASA TN D-6265

INSTRUMENTATION REQUIREMENTS FOR
A FLIGHT REENTRY HEATING EXPERIMENT
AT INTERPLANETARY RETURN VELOCITY

by Elden S. Cornette and Edward M. Sullivan

Langley Research Center

Hampton, Va. 23365



0133072

1. Report No. NASA TN D-6265	2. Government Accession No.	3. Recipient's Catalog No.	
4. Title and Subtitle INSTRUMENTATION REQUIREMENTS FOR A FLIGHT REENTRY HEATING EXPERIMENT AT INTERPLANETARY RETURN VELOCITY		5. Report Date June 1971	
		6. Performing Organization Code	
7. Author(s) Elden S. Cornette and Edward M. Sullivan		8. Performing Organization Report No. L-7574	
		10. Work Unit No. 124-07-18-01	
9. Performing Organization Name and Address NASA Langley Research Center Hampton, Va. 23365		11. Contract or Grant No.	
		13. Type of Report and Period Covered Technical Note	
12. Sponsoring Agency Name and Address National Aeronautics and Space Administration Washington, D.C. 20546		14. Sponsoring Agency Code	
		15. Supplementary Notes	
16. Abstract A study has been made of the flight instrumentation requirements for a ballistic entry simulation of the return of a blunt reentry vehicle from interplanetary flight. It is proposed that total (radiative plus convective) heating rates be measured and that the radiative heating rates be deduced from spectral radiation intensity measurements made with a radiometer mounted inside the spacecraft. Other instrumentation requirements and problem areas involved in the in-flight measurement of the heating environment and heat-shield response are discussed. Areas are pointed out where further development of flight instrumentation and data analysis techniques will be required if the flight experiment is to achieve all proposed experimental objectives.			
17. Key Words (Suggested by Author(s)) Reentry heating Flight instrumentation Radiative heating Spectral radiation Thermal sensors Ablative heat shield		18. Distribution Statement Unclassified - Unlimited	
19. Security Classif. (of this report) Unclassified	20. Security Classif. (of this page) Unclassified	21. No. of Pages 45	22. Price* \$3.00

INSTRUMENTATION REQUIREMENTS FOR
A FLIGHT REENTRY HEATING EXPERIMENT AT
INTERPLANETARY RETURN VELOCITY

By Elden S. Cornette and Edward M. Sullivan
Langley Research Center

SUMMARY

A study has been made of the flight instrumentation requirements for a ballistic entry simulation of the return of a blunt reentry vehicle from interplanetary flight. It is proposed that total (radiative plus convective) heating rates be measured and that the radiative heating rates be deduced from spectral radiation intensity measurements made with a radiometer mounted inside the spacecraft. Other instrumentation requirements and problem areas involved in the in-flight measurement of the heating environment and heat-shield response are discussed. Areas are pointed out where further development of flight instrumentation and data analysis techniques will be required if the flight experiment is to achieve all proposed experimental objectives.

INTRODUCTION

Studies aimed at achieving a better understanding of entry heating in the very high-speed regimes typical of return from planetary missions have been underway for several years (e.g., refs. 1 and 2). These studies have shown that as the entry speed increases above 12 km/sec the radiative heat transfer from the shock heated air increases rapidly and at 15 km/sec can account for over half of the total heat load to the body. Recent results (ref. 3) show that, if an ablative heat shield is used, the radiative heating rate will drive the ablation rate to very high levels which will in turn drive the convective heating rate to a negligible magnitude. In addition, the ablation products have the very beneficial effect of absorbing radiation in certain portions of the spectrum and, hence, the actual radiative heating is significantly below that which would be encountered by a nonablating wall.

All these results are based on calculations made with well-developed flow-field and radiation models. However, all these theoretical models contain some uncertainties, and studies such as those of reference 4 make it apparent that a great deal of experimentation must be done before the calculations can be accepted as reasonably accurate. Most of

these experiments can and should be performed in ground facilities. However, because of facility size, test-gas density, and enthalpy limitations it is believed that a large-scale ballistic flight test will be needed as part of the experimental program. It has been recognized for some time that instrumentation will be one of the key problem areas associated with such a flight test (ref. 5). In order to assist the experimenter who conducts such a flight test, a limited study has been made of the instrumentation which is currently considered essential for a flight test.

The primary purpose of the present paper is to present and discuss those instrumentation and sensor requirements considered essential to the attainment of the experimental objectives and to identify problem areas where further sensor development is necessary. For the purposes of this study it has been assumed that the experimental objectives are to define the heating environment and heat-shield-material response by in-flight measurements, to assess the ability to predict theoretically the heating rates and heat-shield performance, to check the reliability of current ground-facility test results, and to guide future ground tests by exposing any unexpected phenomena which might occur at entry velocities on the order of 15 km/sec.

SYMBOLS

A	projected frontal area of reentry body, cm^2
A_D	area of radiometer detector element, cm^2
A_S	area of radiometer aperture, cm^2
$(BW)_\lambda$	effective bandwidth of radiometer detector element, \AA ($\text{\AA} = 10^{-10} \text{ m}$)
C_D	reentry-body drag coefficient
eV	photon energy, electron volts
g	longitudinal deceleration, g units
h	static enthalpy, cal/g
I_{eV}	spectral radiation intensity, $\text{W}/\text{cm}^2\text{-sr-eV}$
I_λ	spectral radiation intensity, $\text{W}/\text{cm}^2\text{-sr-}\text{\AA}$

i	current developed by radiometer detector element, A
k_λ	radiometer-detector-element calibration factor, A/W
\dot{m}	heat-shield mass-loss rate, g/cm ² -sec
p	pressure, atm (atm = 101 325 N/m ²)
\dot{q}	heating rate, W/cm ²
s	heat-shield surface recession at stagnation point, cm
\dot{s}	heat-shield surface-recession rate at stagnation point, cm/sec
T	temperature, °K
t	elapsed time from initial entry point (Altitude = 122 km), sec
V	velocity, m/sec
W	reentry vehicle weight, N
x	radial distance measured along forebody surface from axis of symmetry of reentry body, cm
y	distance along stagnation streamline measured from body, cm
γ	earth-relative flight-path angle (measured relative to local horizontal; negative downward), deg
δ	shock standoff distance, cm
ρ	density, g/cm ³
τ_λ	spectral radiometer transmission factor
Ω_D	solid angle subtended by radiometer detector element, sr
Ω_S	solid angle subtended by radiometer aperture or window orifice, sr

Subscripts:

C	convective
e	condition at initial entry point (Altitude = 122 km)
edge	condition at edge of boundary layer
eV	spectral quantity in terms of electron volts
R	radiative
stag	condition at stagnation point on vehicle axis of symmetry
w	condition at heat-shield wall
λ	spectrally dependent quantity in terms of wavelength, Å
∞	ambient condition ahead of bow shock
2	condition immediately downstream of bow shock on stagnation streamline

VEHICLE CONFIGURATION, TRAJECTORY,
AND FLIGHT TEST ENVIRONMENT

In order to conduct the instrumentation study, the environment in which the instrumentation would be expected to function must be defined. The results from reference 3 which identifies a spacecraft and a typical ballistic entry trajectory considered to be of interest for a flight test in the interplanetary speed regime were used. The calculated results from this trajectory ($V_e = 14.295$ km/sec, $\gamma_e = -11^\circ$, and $\frac{W}{C_{DA}} = 957.6$ N/m²) have been used as basic input for the instrumentation study.

Vehicle Configuration and Trajectory

The detailed shape and pertinent dimensions of the reentry body chosen for the study are shown in figure 1. The shape of the forebody was that of an ellipsoid of revolution with its minor axis oriented parallel to the free stream. The ellipsoid axes ratio was chosen to be 4:1 so as to provide the desired bluntness and shock standoff distance. The afterbody closure consisted of a cone with a 32.5° angle. For the purpose of this study the maximum diameter of the reentry body was taken to be 1.22 m (4 ft) and the

radius of curvature at the stagnation point was 2.44 m (8 ft). Its maximum allowable weight was assumed to be 1677 N (377 lbf). Of this weight, 890 N (200 lbf) was considered to be instrumentation, data handling, and telemetry equipment. The heat-shield material was chosen to be high-density phenolic and nylon prepared in a 50-50 percent mixture by weight. The specific density of this material is approximately 1.2 gm/cm^3 (75 lbf/ft^3). A hypersonic drag coefficient of 1.5 was used. This drag coefficient was based on available wind-tunnel data.

The entry trajectory parameters are shown in figure 2. Entry is assumed to start at an altitude of 122 km (400 000 ft), a latitude of 7.37° S , a longitude of 16.95° W , and an azimuth angle of 122.87° . Figure 3 shows the longitudinal deceleration history of the reentry package for both the reference (or nominal) trajectory and a more severe overspeed-undershoot trajectory. The velocity, altitude, and deceleration histories were computed on a digital computer utilizing a three-dimensional particle trajectory program which is documented in reference 6. The computations were performed for a rotating, oblate spheroidal earth, with detailed atmospheric data obtained from reference 7.

Flight Test Environment

Figures 4 to 10 show the results of calculations performed to establish values for some of the parameters in which an experimenter would be interested. Figure 4 shows temperature profiles along the stagnation streamline between the body and the bow shock for four times during reentry. Figure 5 shows the time history of the pressure at the stagnation point. Figure 6 shows a history of the stagnation streamline shock standoff distance including the effects of ablation products. The calculated radiative flux histories, both to the edge of the boundary layer and to the ablating wall, are shown in figure 7. The reduction from edge to wall radiative fluxes is due to the presence of ablation products in the boundary layer. The associated ablation rate history for a high density (1.2 gm/cm^3) phenolic-nylon ablation material is shown in figure 8. These high ablation rates, which result from the high radiative fluxes, force the air boundary layer away from the wall. This in turn causes the convective heating rates to be very low as shown by the lower curve in figure 9.

The calculated values shown in figures 4 to 9 were obtained by the methods presented in references 8 and 3. Reference 8 provides the inviscid, radiating air solution for the flow from the shock to the edge of the boundary layer. This solution is used as input to the coupled solution of reference 3 which then calculates conditions at the wall as well as final profiles of radiative flux, temperature, pressure, and species concentrations across the entire shock layer. References 3 and 8 use integral solutions of the flow equations and produce profiles which are somewhat lacking in detail. However, as shown in

reference 9, the integral solutions do produce good average values for the pressure and enthalpy profiles so that the calculated flux values should be accurate.

The radiation model used for the flow-field calculations is that of reference 10 which includes both air and ablation products and gives adequate spectral detail for comparative and flight-test-definition studies. The model of reference 10 does, however, have the shortcoming that it uses line grouping techniques and as a consequence is unsuitable for calculations which will define the instrumentation environment and accuracy requirements. In order to overcome this problem the final calculated profiles of enthalpy, pressure, and species concentration as determined by using the techniques of reference 3 and the radiation model of reference 10 are used in conjunction with the radiation model of reference 11. The resultant spectral radiation intensity plots for four typical times in the trajectory are shown in figure 10. These plots provide detailed estimates of the environment which a spectral radiometer would be required to measure during a simulated earth entry. Figures 4 to 10 establish what can be considered as realistic levels for all pertinent parameters and have been used to provide guidelines for the instrumentation requirements studies.

HEAT-TRANSFER-MEASUREMENT CONSIDERATIONS

Radiative Heating

Figure 7 shows the radiative heating rates predicted for the blunt reentry body and entry trajectory considered herein. The upper curve represents the heat flux at the edge of the inviscid layer. This is approximately the heat flux which would occur at the stagnation point of a body with a nonablating heat shield. The lower curve represents the heat flux predicted for the ablating, phenolic-nylon heat shield considered herein. The difference between the two curves represents the radiation-blocking effectiveness of the relatively cool layer of gaseous ablation products which is expected to be formed near the body surface. It is considered highly important that any reentry heating experiment provide sufficient radiation measurements to confirm this relatively large reduction in radiation to the body. It is assumed that this could be done with the use of an onboard radiometer which would view the radiating gas through an orifice or window in the heat shield. The radiometer should be designed to scan continuously the radiation spectrum. Its output would yield the spectral intensity ($\text{W}/\text{cm}^2\text{-sr-eV}$) of the radiation originating in its field of view and incident at the viewing port. The steradiancy ($\text{W}/\text{cm}^2\text{-sr}$) could then be found by direct integration of the spectral intensity over the wavelength (or photon energy eV) range. The determination of the radiative heat flux (W/cm^2) would require a further integration of the steradiancy over the solid angle of 2π steradians seen by an element of area on the heat-shield surface. However, since the radiometer field of view would necessarily be restricted to a relatively narrow pencil (or ray) extending through

the gas cap, this latter integration could not be performed directly from flight data. The recourse would be to use available radiation models and computer programs appropriately modified such that the theoretical intensity and steradiancy calculations matched those obtained from the measured flight data. Then the calculated radiative heat flux could be accepted as that which existed in flight. As is noted subsequently the spectral intensity measurements would of necessity have limited accuracy in spectral detail. Hence, the deduction of the radiative heating rates must be done with extreme care, especially since no known method exists for measuring radiative heating directly in this environment.

Since the most severe radiative heating would be expected to occur at the stagnation point of the entry vehicle, this area would be of primary interest. However, it is not always feasible to mount instrumentation precisely at the calculated stagnation point. For a perfect, 0° angle-of-attack, ballistic entry trajectory, the stagnation point of the vehicle considered herein would coincide with its axis of symmetry. However, because of spurious body motions and slight construction asymmetries, blunt ballistic entry vehicles seldom fly a perfect 0° angle-of-attack trajectory. Thus it is desirable to provide for instrumentation away from the stagnation point. For a radiometer which viewed the hot gas through the heat shield, an offcenter viewing port would be beneficial in the event that an effluxing-inert-gas radiometer window was used. The effluxing gas would be continuously swept away by the radial flow and, to some extent, by the spinning motion of the entry vehicle. (It has been assumed that the entry vehicle would be axisymmetric and spin stabilized with a spin rate of approximately 180 rpm.)

To investigate the problems that these considerations might impose, 0° angle-of-attack heating-rate calculations were made for the stagnation point and for points located 15 and 30 cm away. The results are shown in figure 11. There is little difference between the heating rates predicted for the stagnation point and the 15-cm point. The associated flow-field calculations indicate that between the stagnation point and the 15-cm point the shock standoff distance and the shock curvature change only slightly. Thus the radiative flux profiles and the radiation spectral details would be expected to have a stagnation-streamline character for a reasonable distance away from the stagnation point. As a result of this investigation it is recommended that a radiometer be mounted reasonably close (within 5 to 10 cm) to the stagnation point and that a detailed analysis be made of the differences between the selected point and the stagnation point.

Two major areas of uncertainty in the radiative heating rate predictions are shown in figures 7 and 11. These are (1) uncertainties in the calculated spectral linear absorption coefficients used in the radiation predictions and (2) uncertainties in the gas-cap temperature profiles. The spectral absorption coefficient at a given point in the gas cap is obtained by summing that for each radiating species which is present. The absorption coefficient for each species is, in turn, determined by summing over all the different

types of radiative transitions which that species can undergo. These calculations involve the use of theoretical models for the various types of radiation transitions as well as the input of much empirical data for each radiating species.

In order to estimate the limit of uncertainty in the calculated flux (because of uncertainty in the spectral absorption coefficients), the absorption coefficients computed for each point in the gas cap were arbitrarily doubled and halved and corresponding new values of the heat flux were computed. These values are indicated by the error band shown on the curve for \dot{q}_{R_w} in figure 7. Doubling the spectral absorption coefficients increases the peak radiative heat flux at the wall by approximately 25 percent, while halving them decreases it by approximately 20 percent. This band is believed to represent reasonable upper and lower limits if the gas-cap temperature profiles are assumed to be determined accurately.

Convective Heating

Figure 9 shows the predicted convective heating rates with and without an ablating heat shield. Presently used theoretical models indicate that, during the critical part of the reentry when the radiative heating rates are large, essentially all of the convective heating component is blocked by the hard blowing of the heat-shield pyrolysis gases. Since such a large reduction in convective heating is indicated for efficient charring ablators, it is considered important that this result be experimentally verified in some manner. Unfortunately, convective heating rates are not directly measurable when large radiative heating rates are occurring simultaneously. However, it should be possible to infer the convective heating component from other measurements with a reasonable degree of accuracy. An approximate value of the radiative flux can be obtained from detailed spectral measurements of the radiation intensity. If a simultaneous, independent measurement of the total (radiative plus convective) heating rate was made, the convective component could be inferred by subtracting the radiative component from the total. If the theoretically indicated reduction in convective heating was indeed achieved, the total flux should be essentially equal to the radiative flux during the critical part of the heat pulse.

Total Heating

In the case of a charring ablator, the development of the appropriate sensors and data analysis techniques required for an accurate assessment of the total heat flux is not a simple problem. In the case of a homogeneous, metallic, heat-sink calorimeter shield, indepth temperature-time-history data can be used in a transient-heat-conduction analysis to determine the exposed surface boundary condition (input total heat flux) with a relatively high degree of confidence. In the case of a charring ablator, however, several

highly coupled ablation mechanisms occur simultaneously and the analysis of the transient, indepth response is complex. In addition to the difficulties involved in making accurate temperature measurements in a charring ablator, the thermophysical properties required for an indepth analysis are generally not known with sufficient accuracy to allow an evaluation of the incident heat flux. To the authors' knowledge, no completely adequate sensors or measurement techniques which would lead to the accurate determination of the total heat flux to a charring ablator have been proposed or successfully demonstrated. Further study and ground-based experimental effort along these lines appear essential since neither the radiative nor convective components of the flux can be measured directly and since both of these inferred values will rely on a total value for validation.

INSTRUMENTATION REQUIREMENTS

Radiation Instrumentation

As previously noted, it has been assumed for the purposes of this work that one of the objectives of the flight test would be to assess the ability to predict theoretically the heating rates and heat-shield performance. Because of the interactions between the ablation products and the convective and radiative heating the measurement of the heating rates will be extremely difficult. It may be necessary to deduce the radiative heating from measurements of the spectral intensity which have been compared to predicted values. Hence, it seems desirable to discuss the radiation instrumentation which has been considered together with the intensity predictions which have been made to date. These predictions are considered typical of the predictions which will be made in the future and will illustrate what is currently conceived to be the best method of interpreting the radiometer data from the spacecraft.

Spectral radiation intensity calculations.- In order to define the sensitivity requirements for an onboard spectral radiometer, predictions of the complete radiation intensity spectra have been made for four times during the reentry heat pulse. These results are presented in figure 10. The solid-line curve in figure 10 presents the intensity spectrum at the wall, that is, the intensity which would be seen by the radiometer, while the dashed-line curve shows the intensity spectrum of the shock heated air incident at the outer edge of the boundary layer. The difference between the two lines is indicative of the predicted blocking effectiveness of the ablation products. The four times chosen and the total radiative flux to the wall are shown by the circle symbols on the stagnation-point heat-flux curve \dot{q}_{R_w} plotted in figure 7. The associated flight conditions and other pertinent parameters are given in table I.

The detailed intensity spectra shown in figure 10 were computed by using the SPECS radiation code (ref. 11). Two features which influence instrumentation considerations are apparent in figure 10. First, note the significant reduction in radiation intensity at

the wall in the spectral range above 6 eV. Most of this reduction (particularly above 8 eV) is attributed to the absorption of radiation by the ablation products in the boundary layer. As shown in reference 3, this reduction can amount to 20 to 50 percent of the radiative flux reaching the edge of the boundary layer. Because of the importance of the blocking of radiation by ablation products in this spectral region it is important to be able to make measurements as far into the ultraviolet as possible. Because of the practical problems of making measurements in the far ultraviolet, the upper limit should be chosen carefully. At the present time a limit of 11 or 12 eV is believed to be adequate. The second important feature is the group of lines in the infrared between 1 and 2 eV. These lines are attributed primarily to the nitrogen atom (20 lines), the oxygen atom (19 lines), and the nitrogen positive ion (9 lines). The maximum intensity of many of the lines in this group is predicted to be as much as two orders of magnitude above the general background continuum. These lines represent the most intense radiation seen in the entire spectrum for times near peak heating. The envelope of maximum line intensities provides a basis for setting the radiometer maximum sensitivity requirements in this spectral region.

Radiation measurement requirements. - The intensity calculations and spectral features previously discussed provide a basis for determining the measurement ranges and spectral coverage desired in a flight experiment. Accordingly, an estimated maximum measurement range envelope was constructed by determining, in each spectral region, the maximum intensity indicated by the spectra presented in figure 10 and then arbitrarily multiplying these maximums by a factor of 5. The resulting upper envelope is shown in figure 12. Note that this upper envelope includes the upper bound produced when the ablation products are assumed to be completely ineffective in blocking the incident radiation.

Although the radiation spectra shown in figure 10 indicate that the intensity seen by the radiometer could vary over several orders of magnitude for one complete scan across the spectrum, much of this variation is well below the level of interest and is completely negligible. To establish a lower limit of interest, any given spectral intensity level must be interpreted in terms of the corresponding spectral flux to the body. Accordingly, the flux spectra which correspond to the intensity spectra shown in figure 10 have been calculated. The flux spectrum presented in figure 13 for the time of peak heating is typical. Except for a few isolated line peaks, the spectral flux (shown in fig. 13) is indicated to be less than $1 \text{ W/cm}^2\text{-eV}$ (i.e., $\log_{10}(\dot{q}_{\text{ReV}}) < 0$) for all of the spectra above 8 eV. If the sensitivity threshold of the radiometer could be maintained at an intensity level of approximately $0.1 \text{ W/cm}^2\text{-sr-eV}$ ($\log_{10}(I_{\text{eV}}) \approx -1$), then the maximum undetected flux would be less than $1 \text{ W/cm}^2\text{-eV}$ and would indeed be negligible. Furthermore, if the

vacuum ultraviolet radiation is absorbed by the ablation layer as predicted, the radiation in the spectrum above 8 eV would generally be below the sensitivity threshold of the radiometer.

Another reason for attempting to maintain a relatively low sensitivity threshold is the possibility of acquiring early reentry data at high altitudes and low densities where nonequilibrium radiation effects are expected to predominate. Flight data are needed in this area to corroborate ground-based experimental findings and possibly provide a basis for a theoretical approach to this facet of the radiative heating problem. In any event, an intensity level of $0.1 \text{ W/cm}^2\text{-sr-eV}$ is considered to be a lower limit of interest, and a corresponding lower envelope is shown in figure 12.

Radiometer performance.- After the expected radiation intensity levels have been calculated and the desired measurement ranges established, the radiometer performance requirements can be specified. By realizing that some goals cannot be achieved with present state-of-the-art components and design practices, an effort will be made to define some of the practical limitations and anticipated problem areas. Present limitations will be discussed in terms of their effect on the usefulness of the data and the ultimate achievement of the experimental goals. Areas where further instrument development appears justified or is definitely required will be pointed out.

The overall performance of the radiometer instrument can be evaluated in terms of such criteria as dynamic range, spectral coverage, resolution, data or scan rate, signal-to-noise ratio, sensitivity, reliability, and the general appearance and usefulness of the resulting data.

Dynamic range.- The dynamic range of a radiometer is defined as the difference between its threshold level of detectability (the lowest intensity level which can be distinguished from the background noise) and its saturation limit (the highest intensity level at which an increase in source intensity is accompanied by a reasonable increase in signal output). Maintenance of a large dynamic range at all wavelengths is desirable to insure that the instrument is capable of monitoring the complete variation of intensity with time during entry. Based on the intensity spectra shown in figure 10, it is evident that, if the threshold intensity level could be maintained at approximately $0.1 \text{ W/cm}^2\text{-sr-eV}$ (i.e., $\log_{10}(I_{\text{eV}}) = -1$) then a dynamic range of five decades (orders of magnitude) would cover the maximum expected intensities over most of the spectra. Many practical design considerations limit the dynamic range which can actually be achieved. The dynamic range will depend upon the particular detector element or elements chosen as well as the associated electronic signal-amplification circuitry. In addition, the dynamic range will vary with wavelength because of differences in detector sensitivity, noise level, and other factors. Figure 12 indicates that a dynamic range of

five decades would be sufficient for all of the spectra except for the possible clipping of the tops of some of the atomic lines located in the infrared below 2 eV. If necessary, this loss could be tolerated since the verification of their existence would be established. However, it would be desirable to measure their strengths and thereby gain an important verification of preflight predictions.

Window considerations.- The feasibility of making in-flight measurements of the radiation in the wavelength range below approximately 2000 Å (photon energies greater than 6.2 eV) is open to question. All known optical window materials which could withstand the severe external heating environment for any significant length of time are nontransparent in this wavelength region. There are window materials available which will transmit satisfactorily at wavelengths as low as approximately 1100 Å (11.27 eV), but these materials are known to be highly sensitive to the type of environment to which they would be subjected. Apparently the most satisfactory window material would be an optical-grade, clear fused silica (quartz). The practical minimum wavelength at which reliable measurements could be made through this type of window is approximately 3000 Å (4.13 eV). The better grades of optical quartz will transmit satisfactorily at somewhat shorter wavelengths so long as the window temperature is maintained at or near room temperature. However, their transmissivity at wavelengths shorter than 3000 Å decreases quite rapidly with increased window temperature. The reduction and analysis of data obtained at these shorter wavelengths would require that large corrections be made for the reduced transmissivity of the window. An accurate knowledge of the temperature distribution through the window as a function of time during entry is essential to make these corrections. Since window temperatures cannot be satisfactorily measured in flight, the only recourse would be the analytical prediction of the temperature distributions. This procedure appears feasible for wavelengths above 3000 Å where only small changes in transmissivity occur but is not considered sufficiently reliable for the spectral region below 3000 Å where transmission decreases rapidly.

Window materials characteristically have very low values of thermal conductivity and thus are not good heat-sink materials. When heated, their surface temperature rises rapidly while their interior remains relatively cool. Even though the melting temperature of fused quartz is relatively high (1800^o to 2000^o K), its time to surface melt would be relatively short for the heating rates anticipated. If the convective heating component is indeed reduced by the hard blowing of ablation products as predicted by theory, then the maximum useful lifetime of a fused-quartz window is estimated to be on the order of 5 seconds. This estimate is based on protecting the window and not exposing it until the critical portion of the heat pulse near peak heating. Furthermore, if the window was not contaminated by ablation products, it could be expected to be partly transparent for a short time after surface melting begins. However, the short wavelength end of its transmission spectrum would be seriously degraded.

The major factor which makes the use of any solid window undesirable is the loss of the ability to make radiation measurements in the important wavelength range below 2000 Å. It has been suggested that an effluxing-inert-gas window be used to cover the vacuum ultraviolet region of the spectrum; that is, the wavelength dispersion and detector element or elements would be located in a cavity and view the radiating gas cap through a small orifice in the heat shield. A constant, small efflux of an inert gas, such as helium (which has negligible absorption in the spectral range of interest), would be maintained through the orifice to prevent external gases from entering the cavity. The inert-gas flow rate would be controlled by a flow regulator designed to maintain a small positive pressure differential between the cavity internal pressure and the external surface pressure. Limited breadboard tests have indicated that satisfactory off-the-shelf flow regulators can be obtained which will maintain the desired pressure differential for external orifice diameters up to 0.48 cm (3/16 inch) and for rather severe step function changes in the external pressure. The required onboard gas storage capacity does not appear to be prohibitive. However, this gas-window technique remains essentially unproven, and further development and testing would be required before it could be incorporated into a flight radiometer design.

Resolution.- It is not considered feasible to attempt to design a flight spectrometer with sufficient resolution to distinguish individual atomic lines. Such an instrument would not be justified on the basis of the experimental objectives discussed herein. Current studies indicate, however, that an instrument capable of defining individual molecular bands or line groups could be designed using current state-of-the-art technology for a large part of the spectrum. An instrument with a resolution of 50-Å or less was originally assumed to be sufficient and practical for those regions of the spectrum where the greatest detail was desired. In order to check this assumption quantitatively, a computer program was written to pass an idealized, rectangular, band-pass numerical filter across the detailed intensity spectra shown in figure 10. The program was written such that any constant filter bandwidth could be selected and the filter could be moved across the spectra in discrete steps of any chosen size. The results of passing a 50-Å filter across the spectrum in discrete 50-Å steps is shown in figure 14 by the solid-line curve. This smeared spectrum is believed to represent the resolution which could be obtained by dispersing the incoming radiation over a linear array of solid-state detector elements sized such that each element detected a 50-Å band. Apparently such an instrument would adequately detect the existence of significant line groups and strong band heads as well as any sharp variations in the underlying continuum. The results obtained by using a 25-Å filter with 25-Å steps is shown by the short-dashed-line curve in figure 14 and a 100-Å filter with 100-Å steps is shown by the long-dashed-line curve. A resolution of 25-Å would be highly desirable and would provide many more spectral points for verification of the preflight analysis. The detail from a 100-Å radiometer would be very poor.

The authors feel that a 100-Å radiometer would be inadequate and that further studies should be made to establish the need for a resolution better than 50 Å.

Another possibility, which has not been investigated, is that of using a radiometer with 50-Å, or less, resolution in the range to 6 or 8 eV and a much wider band resolution over the remainder of the spectrum. Such a possibility should be explored prior to the design of the flight instrument.

Scan rate.- The radiometer spectral scan rate should be high enough such that the intensity spectrum would not change significantly during one complete scan. A rate of 10 scans per second should be satisfactory. A radiometer designed with no moving parts would be highly desirable. This design would considerably increase the instrument reliability and eliminate any inertia or g-loading effects during entry deceleration. One design concept which appears feasible from this standpoint is the use of a concave, reflecting grating as a dispersion element followed by an array of miniature, solid-state detector elements which could be scanned electronically. The feasibility of such an instrument for application in the vacuum ultraviolet is discussed in reference 5.

Candidate solid-state detector elements are photodiodes, phototransistors, and photoconductors. Linear arrays of semiconductor photodetectors have been successfully used in the visible region of the spectrum for some time. By using current fabrication techniques, the elements can be made very small in size and packaged in linear arrays of 100 or more per cm. An attractive design feature of currently available solid-state image scanners is the use of electronic switching from a large number of photosensitive elements to a single output terminal. Such switching circuits have been fabricated in integrated circuits of small volume and power consumption. It is believed that much of this technology should be applicable in the design of a flight radiometer for reentry heating measurements.

Detector sensitivity.- To determine the spectral distribution of the energy radiated into an instrument of aperture area A_S and in which the detector subtends a solid angle Ω_D , simply compute the product $I_\lambda \Omega_D A_S$ (W/Unit wavelength), where I_λ can be obtained from the intensity spectra presented in figure 10. For a system in which the field of view is completely filled by a uniform source of intensity I_λ , the equation for the current developed by a detector element is

$$i = I_\lambda (BW)_\lambda k_\lambda \tau_\lambda \Omega_D A_S$$

The factors $(BW)_\lambda$, k_λ , τ_λ , Ω_D , and A_S are quantities determined by the specific radiometer design. The product $\Omega_D A_S$ can be replaced by the product $\Omega_S A_D$ where Ω_S is the solid angle determined by the field of view of the detector (i.e., subtended by

the radiometer aperture or window orifice) and A_D is the area of the detector element. Thus the maximum sensitivity (current) would be obtained with a large detector element having a large solid angle of view. Such a detector would, however, experience a larger heat flux and temperature rise so that some tradeoff would be necessary if the detector was limited to a relatively narrow temperature range. Fortunately, Ω_S and A_D (or Ω_D and A_S) are geometric design variables which are under the designer's control. Thus some latitude is available in establishing detector operating current and temperature levels through these design variables.

The effective bandwidth $(BW)_\lambda$ would depend upon the resolution obtained in the specific radiometer design. For a design in which the incoming radiation was dispersed over a linear array of solid-state detectors, the value of $(BW)_\lambda$ for each individual detector element would depend upon the actual physical width of the detector element. The value of the calibration factor k_λ would depend upon the particular detector element chosen. No single detector would operate satisfactorily over the entire spectrum. In order to cover essentially all of the spectrum, several different types of detectors would be required (each covering that portion of the spectrum in which it operated the most efficiently). In general, the sensitivity of any one type of detector is not constant but varies considerably with wavelength. Thus adequate detector calibration procedures are important. It is also important that provisions be made to insure that the calibration factor does not change during launch delays or during the downrange coast phase of the flight.

The value of the spectral transmission factor τ_λ would depend upon the optics of the system as well as the wavelength dispersion element. The requirement to make measurements in the vacuum ultraviolet would rule out a prism as a dispersion element, at least in the vacuum ultraviolet region of the spectrum. Careful attention would be required to eliminate scattered light and, in the case of grating instruments, the interference from second and higher order contributions. Selective filters are available for this purpose and could be used for regions of the spectrum other than the vacuum ultraviolet.

Several questions relative to the application of solid-state detectors in the vacuum ultraviolet have yet to be answered. Factors which require further experimental investigation include absolute sensitivity calibration in the vacuum ultraviolet, threshold level of detectability, dynamic range, temperature effects, fatigue or memory effects, and the effect of atmospheric and environmental contamination. The temperature sensitivity of the detector elements would have to be defined to determine whether an onboard cooling system would be required.

Ablation Instrumentation

The boundary-layer portion of the flow field will be dominated by the products of ablation during the time of peak heating. It has been predicted that the large ablation rates will prevent convective heating from being important and the ablation products will block a significant fraction of the radiative heating. In addition, the ablating surface will reradiate a significant fraction of the incident heat load. Thus in order to establish a correct energy balance for any time during the flight it is necessary to know the surface temperature, the mass-loss rate, and the condition of the ablation products as they enter the boundary layer. Experience has shown that none of these parameters, with the possible exception of the surface temperature, can be measured directly. The mass-loss rate must be deduced from measurements of the char surface and pyrolysis zone locations. The actual chemical state of the exiting gas cannot be determined by any methods currently known. The measurements which can be made and the need for other information will be discussed.

Temperature measurements.- Instantaneous depthwise temperature distribution through the heat-shield material can be determined by cross-plotting temperature-time-history data obtained at several different depths. Since the char formed by the decomposing heat shield would be expected to be essentially pure carbon, the surface temperature would be expected to approach the sublimation temperature of carbon. Although carbon sublimates at a varying rate over a fairly large temperature range (depending upon the pressure), surface temperatures as high as 3000° to 3500° K could be expected.

Figure 15 shows the predicted temperature-time history at the exposed surface of a phenolic-nylon heat shield during a ballistic entry such as that considered herein. These calculations indicate that, during the radiative heat pulse, temperature rise rates on the order of 300° K per second could be expected until the sublimation temperature was reached and a relatively steady surface recession was established.

The obvious and best sensor for making in-flight temperature measurements is the thermocouple. Although thermocouples cannot be expected to measure accurately the extremely high temperatures near the heat-shield surface, their proper use should provide temperature-time histories at several depthwise locations in the lower temperature region of the char layer, pyrolysis zone, and virgin material. These data could be used as matching criteria in indepth heat-shield-material analysis programs. Once the measured temperature-time histories are matched by the analytical program, the program could then be used to extrapolate the temperature distribution to the surface with some degree of confidence.

There are many possible problems associated with the use of thermocouples in ablation materials. Their successful application is highly dependent upon the details and techniques of installation. (See refs. 12 and 13.) The detailed design requirements for

the optimum sensor for a particular application will vary with the specific material under consideration. Care must be taken to obtain and maintain good thermal contact and to avoid the effects of material expansion during heating. Since most chars are good electrical conductors, good high-temperature electrical insulation must be provided for the thermocouple leads to prevent electrical shorting through the char and premature malfunctions. Although thermocouples (such as tungsten-rhenium combinations) have been successfully calibrated to temperatures higher than 3000° K, the best available electrical insulation materials begin to break down at temperatures around 2500° K. Thus good electrical insulation techniques may be the factor which limits the maximum usefulness of thermocouples in charring ablaters.

Since ablation materials have very low values of thermal conductivity compared to those of thermocouple wire, thermal sensors must be carefully designed to avoid large errors in the temperature measurements owing to heat conduction along the thermocouple leads. The results of references 12 and 13 indicate that errors of this type can be greatly reduced by using small-diameter lead wire and routing short lengths of the sensor lead wire along the isothermal plane of the hot junction. Several thermocouple installation techniques have been tested and appear to be satisfactory in this respect.

Surface-recession and mass-loss rates.- Although total heat-shield surface recession could be determined by examination of the recovered reentry package, it is considered essential to make sufficient in-flight measurements to be able to estimate the surface-recession rate and mass-loss rate during the time near peak heating when the ballistic entry experiment should closely simulate the conditions of a manned lifting entry. Because of the extremely high temperatures attained at the char surface, any sensor designed to make in situ measurements of the surface location would have to withstand an extremely severe environment. Continuous measurements of the char surface location would be highly desirable. However, a history of the surface location could be adequately determined from a series of point measurements (i.e., measurements of the time at which the char surface passed a series of known points). Such measurements could be made with several spring-wire sensors used in a gang installation as described in reference 14.

Figure 16 shows the surface recession and surface-recession rates predicted for a 1.2-gm/cm^3 phenolic-nylon heat shield and the ballistic entry considered herein. The calculations indicate that significant surface recession would occur over a relatively short time period of approximately 12 seconds. A total heat-shield surface recession of slightly less than 0.5 cm would occur during this time. The surface-recession rate would reach a maximum of approximately 0.064 cm/sec near the time of peak heating. These results indicate that meaningful point measurements of the surface location could only be made by sensors having their trigger ends located at some point within the first half centimeter of

heat-shield depth. At least two such measurements are required to establish a recession rate. However, three or four measurements at a given radial station would be required to provide confidence in the reliability of the sensors. Somewhat redundant installations at different azimuthal and radial stations would be desirable. In these installations the sensors could be staggered in depth so that recession-rate determinations could be made for three or four times during the sensible heat pulse. Sensor-design depth locations could be chosen from a surface recession prediction such as that shown in figure 16. By using the surface-recession curve, the depthwise spacing which would be required between any two sensors to have them trigger at definite time intervals (say 2 seconds apart) could be determined. Considerably wider spacing would be required for times near peak heating than for times early and late in the heat pulse.

The local mass-loss rate can be estimated from measurements of the location of the exposed char surface and the location of the char—virgin material interface as a function of time. These two measurements define the char thickness. When these data are coupled with a knowledge of the composition and density of the char and the undegraded heat-shield material, the mass-loss rate can be determined. The problem here is the fact that there is no clear-cut char—virgin-material interface but rather a pyrolysis zone which changes character with time during reentry. Probably the best indication of the time of passage and character of the pyrolysis zone could be obtained from thermocouple data. It should be possible to use both the surface-recession measurements and indepth thermal-response data as simultaneous forcing functions or boundary conditions (constraints) to be applied to an indepth material-response computer program which would yield mass-loss rates.

Ablation mechanisms and pyrolysis gas state.- The known ablation mechanisms which occur within the material include the decomposition of the virgin material to pyrolysis gases and a carbonaceous char layer, heat conduction, heat storage, and sensible heating of the pyrolysis gases during their finite residence time in the porous char layer. Since the pyrolysis gases must flow outward against very large temperature gradients in the char layer, their total enthalpy is increased both by virtue of their temperature rise and their exit velocity. Other possible subsurface mechanisms have been postulated and are believed to occur in varying degrees depending upon the severity of the heating environment, the char thickness, the exact composition of the material involved, and other factors. These mechanisms include any homogeneous chemical reactions which take place among the pyrolysis gas species while they are still in the char layer. These cracking reactions are generally endothermic and thus constitute a heat dissipation mechanism. The results of analytical calculations reported in reference 4 indicate a very large difference in the total heat absorbed per pound of heat-shield material dependent upon whether the upper bound condition (complete thermal and chemical equilibrium

at the char surface temperature as the result of infinitely fast gas reaction rates) or the lower bound condition (no chemical reactions, i.e., the pyrolysis gas composition is frozen at that of the pyrolysis temperature) is assumed. In any actual situation the composition of the pyrolysis gases in the char layer and issuing from the char surface might be anywhere between these bounds. Thus the problem would be one of nonequilibrium chemistry with all of its attendant difficulties.

The probability of indepth heterogenous reactions between the pyrolysis gases and the solid char also exists. The pyrolysis gases may either erode the porous char or deposit additional residue upon it (coking reactions). Homogeneous chemical reactions within the solid char could also occur to change the nature of the char if it contained constituents other than pure carbon. Aside from these purely chemical mechanisms, at extremely high heating rates the char might be subject to separation, collapse, or fragmentation because of severe mechanical and thermal stresses. These stresses are produced by the very large pressure and temperature gradients which must be supported by the char layer.

Certain very important ablation mechanisms occur essentially at the exposed char surface; namely, the emission of radiant energy by the hot char surface, the reflection or scattering of incident radiation from the hot gas cap, heterogeneous oxidation reactions between the char and the free-stream oxygen which diffuses to the surface, and the direct sublimation of the solid char to its gaseous species. Also mechanical erosion or spallation of the char surface has been observed at high values of total pressure.

In addition to the previously mentioned mechanisms other significant and unexpected ablation phenomena might occur at interplanetary return velocities. For example, possibly the melting of refractory fibers or inorganic filler materials could produce enough liquid phase material to partly or intermittently seal the porous char surface, thus momentarily trapping the pyrolysis gases in the char layer. The subsequent internal pressure buildup and local boiling action could produce a highly undesirable mode of local char failure. This surface sealing phenomenon and other material performance anomalies have been observed in ground-facility tests. The problem of analytically calculating the heat-shield-material response is complicated by the fact that most of the known ablation mechanisms occur simultaneously and are highly coupled. Considerably more experimental study is needed to establish a priority among the various ablation mechanisms and to generate a greater degree of confidence and uniformity in the theoretical ablation models currently used.

Radar Coverage and Tracking Instrumentation

The assumption has been made that the entry package would be axisymmetric, that it would be spin stabilized, and that it would fly a 0° angle-of-attack trajectory with the

parameters shown in figure 2. The entry trajectory actually flown is never identical to the prescribed trajectory because of the mechanical problems in spacecraft fabrication, tolerances on attitude at staging, deviations in the atmospheric model, and so forth. A brief study has been made of the sensitivity of the calculated heating rates to variations in velocity at the time of peak heating. The results indicate that the calculated heating rate varies by approximately 2 percent for each 30.48-m/sec variation in velocity. Thus the actual trajectory flown must be determined with a high degree of accuracy.

Radar coverage.- The reentry trajectory actually achieved during a flight experiment is normally determined by the use of data obtained from ground-based tracking radars. These radars provide data in the form of range, azimuth, and elevation of the reentry body from known ground stations as a function of time. These data are then converted to the flight parameters of altitude, velocity, and flight-path angle. When these flight parameters are coupled with the prevailing atmospheric conditions (temperature, pressure, and density), the basic experimental conditions are determined.

Higher velocities associated with reentry at interplanetary return speeds will considerably increase the difficulty in acquiring and maintaining the reentry package target on the tracking radar. An onboard beacon transmitter to assist in radar tracking is considered essential. It is desirable to acquire the target as early as possible. Acquisition of target prior to separation of the reentry package from the velocity package will require that the beacon transmitter feed an antenna located on the reentry-package-velocity-package adapter prior to separation and then switch to one located on the reentry-package afterbody after separation.

Since the reentry package cannot be continuously tracked by radar because of the radio-frequency blackout phenomenon, reconstruction of that portion of the reentry trajectory lost during blackout would be necessary. This reconstruction can be done by a computer simulation using the last good radar data prior to blackout as the initial conditions. Thus several sources of radar data should be available for comparison in selecting these initial conditions. It is assumed that final recovery of the reentry package would be an experimental ground rule. This recovery of the reentry package should provide a known final impact point which, when combined with radar data obtained after blackout, would serve as additional boundary conditions on the trajectory simulation. The use of a ballistic rather than a lifting entry trajectory considerably simplifies the computer simulation and a very accurate reconstruction would normally be expected.

If a ballistic experiment of the type envisioned was to be flown, it would seem that the major uncertainty in gas-cap temperatures could be attributed to uncertainties in the actual velocity and altitude at a given time during reentry. In order to estimate the influence of such an error it was assumed that the velocity was actually 30.5 m/sec (100 ft/sec) higher or lower than the nominal value at the time of peak heating. These

limits were selected on the basis of estimates of radar-tracking accuracy. The calculated heating rate was found to range from 2 percent above nominal to 2 percent below nominal. When the velocity error limits were increased to ± 152.4 m/sec (± 500 ft/sec), the heating rate varied by 10 percent above and below nominal. It is evident that the velocity must be known very accurately if the validity of the heat-transfer calculations is to be established with a high degree of accuracy.

Body-motion instrumentation.- The body spin rate and any spurious body motions which occur during reentry should be monitored by accelerometers and rate gyros mounted along the longitudinal (roll), transverse (pitch), and normal (yaw) axes of the reentry package. These instruments are considered to be off-the-shelf items and should require no special development. The only consideration would be the appropriate choice of the maximum measurement ranges for these instruments and the data sampling rates necessary to define any body motions. The longitudinal deceleration curve for the reference trajectory ($V_e = 14\,295$ m/sec (46 900 ft/sec); $\gamma_e = -11^\circ$) used in this work is shown in figure 3. Also shown is that for a somewhat more severe, overspeed ($V_e = 14\,630$ m/sec (48 000 ft/sec)) and undershoot ($\gamma_e = -12^\circ$) condition. This tolerance for the initial entry velocity and flight-path angle is conservative and well within current guidance and control capability.

Based on the results shown in figure 3, a longitudinal accelerometer with a range from 0 to -100g would be capable of recording the maximum deceleration with a 20- to 40-percent margin. Since the accuracy of an accelerometer with such a high range is relatively low at the lower acceleration levels, a second longitudinal accelerometer with a range from -10 to 10g would be desirable. Based on past flight experience, the maximum transverse and normal accelerations would not be expected to exceed 10 percent of the maximum longitudinal acceleration. Thus a range from -10 to 10g should be sufficient for accelerometers oriented along these two axes.

The range of the roll-rate gyro should be sufficient to verify the spin rate used to stabilize the reentry package plus any roll perturbations due to unwanted body motions. If a spin rate of 3 rps plus a 10-percent perturbation is assumed, a maximum roll-rate range of 20.72 rad/sec would be expected. A roll-rate gyro with a range from 0 to 25 rad/sec should be sufficient. The maximum range of the pitch and yaw rates would not be expected to exceed 8 rad/sec unless unusually severe body motions involving angle-of-attack excursions greater than 35° were encountered. This estimate is based on the rates measured during the Project Fire reentry heating experiments (refs. 15 and 16) where relatively large body motions occurred.

Several methods which have been used to reconstruct reentry body motions from accelerometer, rate-gyro, and other data sources are presented in references 15 and 16. If a single-layer, charring-ablation heat-shield material was employed, large mass

unbalances (such as those which can occur on melting, metallic heat shields) would not normally be expected. No large disturbing aerodynamic moments should be produced by the heat-shield mass loss. Any unsymmetrical spallation of the char layer should produce only small body-motion disturbances or a small nonzero trim angle.

The onboard instrumentation required for trajectory and body-motion analysis is currently available as off-the-shelf items. The reconstruction of the actual reentry trajectory and the definition of any spurious body motions would present no particular problem in the experiment design.

CONCLUDING REMARKS

A study has been made of the flight instrumentation requirements for a ballistic entry simulation of the return from interplanetary flight. The study assumed a ballistic entry trajectory with an initial entry velocity of 14.295 km/sec (at an altitude of 122 km), a ballistic parameter of 957.6 N/m², and an initial entry angle of -11°. The entry vehicle considered had a blunt forebody shaped like that of an ellipsoid of revolution, with a 4:1 axes ratio, and a 32.5° conical afterbody. The calculated values show that the radiative heating rate is large enough to cause ablation rates which will in turn reduce the convective heating rates to negligible values.

In this environment the measurement of heating rates is extremely difficult. There is no known method of measuring either the convective or radiative heating directly. It is proposed that the total (radiative plus convective) heating rates be measured and that the radiative heating rates be deduced from spectral radiation intensity measurements made with a radiometer mounted inside the spacecraft.

In order to achieve the experiment objectives, radiation instrumentation of a very high quality would be required. Radiative heating rates should be deducible with a high level of confidence. It is also of primary importance that spectral radiation measurements be made as far as possible into the ultraviolet (at least to 12 eV) since a considerable amount of the gas-cap radiation is predicted to occur in this part of the spectrum. Such measurements could not be made if a solid radiometer window was used. It is thus proposed that an effluxing inert-gas window be used. A spectral resolution of 50 Å would give acceptable results, but a somewhat better resolution would be desirable.

In-flight measurements of heat-shield response are considered important. Ablation instrumentation will be required to evaluate the heat-shield mass-loss rate and surface-recession rate. It is proposed that conventional thermocouple and spring-wire instrumentation would be acceptable. The problem of determining the chemical state of the heat-shield pyrolysis gases has not been solved. This problem will require rather extensive ground tests and empirical correlations which can be applied to the flight test data.

Reentry vehicle tracking can be accomplished with existing radars but the unusually high entry velocity may impose some serious target acquisition problems. Body motions and attitude can be determined from accelerometer and rate-gyro data. The anticipated ranges are nominal and it is believed that this type of instrumentation is available off the shelf.

Langley Research Center,
National Aeronautics and Space Administration,
Hampton, Va., March 24, 1971.

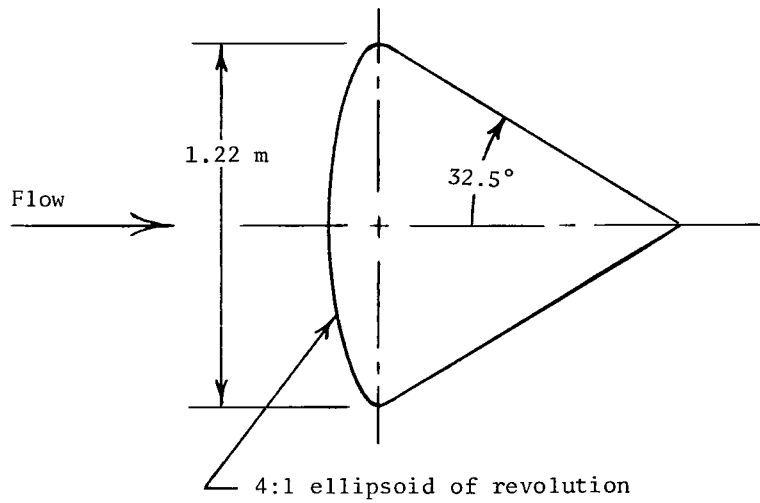
REFERENCES

1. Sohn, Robert L: Manned Mars Trips Using Venus Swingby Modes. Third Manned Space Flight Meeting, Amer. Inst. Aeronaut. Astronaut., Nov. 1964, pp. 330-338.
2. Roberts, Leonard: Entry Into Planetary Atmospheres. Astronaut. Aeronaut., vol. 2, no. 10, Oct. 1964, pp. 22-29.
3. Smith, G. Louis; Suttles, John T.; Sullivan, Edward M.; and Graves, Randolph A., Jr.: Viscous Radiating Flow Field on an Ablating Blunt Body. AIAA Paper No. 70-218, Jan. 1970.
4. Coleman, W. D.; Hearne, L. F.; Lefferdo, J. M.; and Vojvodich, N. S.: A Study of the Effects of Environmental and Ablator Performance Uncertainties on Heat Shielding Requirements for Blunt and Slender Hyperbolic Entry Vehicles. AIAA Paper No. 68-154, Jan. 1968.
5. Ohlhaber, Ronald L.; Betz, Howard T.; and Klugman, Earl H.: Advanced Evaluation of Vacuum UV Detector-Spectroscopy Systems for Capsule Reentry Measurements. Rep. V6098 (Contract No. NAS 1-8992), IIT Res. Inst., Apr. 1970. (Available as NASA CR-111776.)
6. Dennison, A. J.; and Butler, J. F.: Missile and Satellite Systems Program for the I.B.M. 7090. Tech. Inform. Ser. No. 61 SD 170, Missile and Space Vehicle Dep., Gen. Elec. Co., Feb. 1962.
7. Anon.: U.S. Standard Atmosphere, 1962. NASA, U.S. Air Force, and U.S. Weather Bur., Dec. 1962.
8. Suttles, John T.: A Method of Integral Relations Solution for Radiating, Nonadiabatic, Inviscid Flow Over a Blunt Body. NASA TN D-5480, 1969.
9. Falanga, Ralph A.; and Sullivan, Edward M.: An Inverse-Method Solution for Radiating, Nonadiabatic, Equilibrium Inviscid Flow Over a Blunt Body. NASA TN D-5907, 1970.
10. Wilson, K. H.: RATRAP - A Radiation Transport Code. 6-77-67-12, Lockheed Missiles & Space Co., Mar. 14, 1967.
11. Thomas, M.: The Spectral Linear Absorption Coefficients of Gases - Computer Program SPECS (H189). DAC-59135, Missile & Space Syst. Div., Douglas Aircraft Co., Inc., Dec. 1966. (Revised May 1967.)
12. Dow, Marvin B.: Comparison of Measurements of Internal Temperatures in Ablation Material by Various Thermocouple Configurations. NASA TN D-2165, 1964.

13. Brewer, William D.: Effect of Thermocouple Wire Size and Configuration on Internal Temperature Measurements in a Charring Ablator. NASA TN D-3812, 1967.
14. LeBel, Peter J.; and Russell, James M., III: Development of Ablation Sensors for Advanced Reentry Vehicles. 20th Annual ISA Conference Proceedings, Vol. 20, Pt. II, Preprint No. 17.18-5-65, c.1965.
15. Woodbury, Gerard E.: Angle-of-Attack Analysis for Project Fire 1 Payload Reentry Flight. NASA TN D-3366, 1966.
16. Scallion, William I.; and Lewis, John H., Jr.: Body Motions and Angles of Attack During Project Fire Flight II Reentry. NASA TN D-4183, 1967.

TABLE I. - REENTRY CONDITIONS AND ENVIRONMENTAL PARAMETERS
FOR WHICH DETAILED RADIATION INTENSITY SPECTRA
HAVE BEEN CALCULATED

t, sec	Altitude, km	V, m/sec	T ₂ , °K	P ₂ , atm	ρ ₂ , gm/cm ³	ρ ₂ /ρ _∞	h ₂ , cal/gm	δ _{stag} , cm	\dot{m}_w , gm/cm ² -sec	\dot{q}_{Cstag} , W/cm ²	\dot{q}_{Rstag} , W/cm ²
24	63.353	13650	13149	0.3503	3.452 × 10 ⁻⁶	17.040	22213	8.059	0.0222	12.0	1183
26	59.306	13169	13177	.5370	5.514	16.504	20679	8.498	.0435	5.4	1687
28	55.510	12458	12933	.7612	8.453	15.950	18511	8.700	.0571	2.0	1988
30	52.021	11499	12281	.9826	12.386	15.403	15778	8.797	.0442	8.1	1702



$$\frac{W}{C_D A} = 957,6 \text{ N/m}^2$$

Figure 1.- Reentry-body geometry.

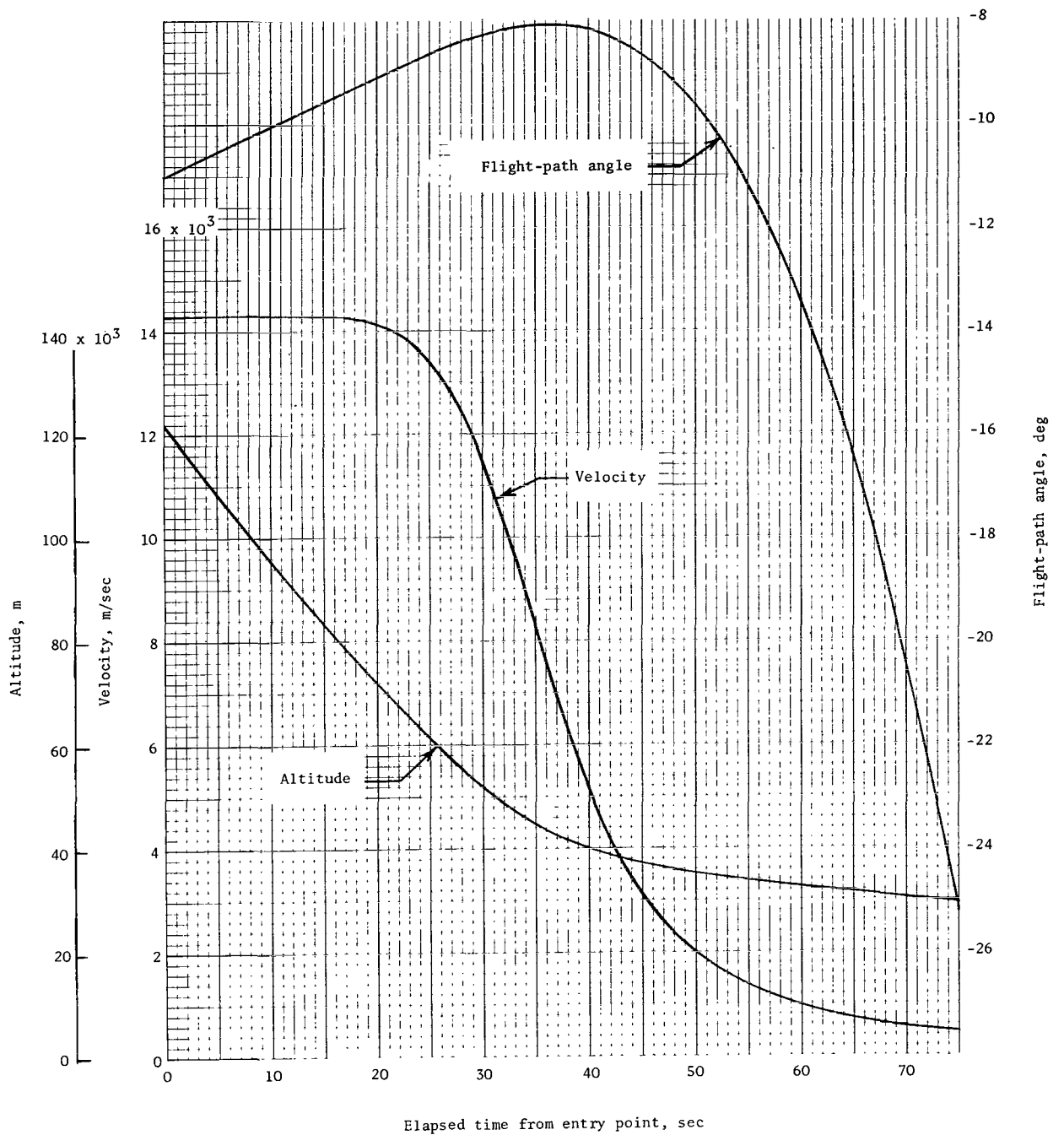


Figure 2.- Entry trajectory parameters for reference trajectory ($W/C_{DA} = 957.6 \text{ N/m}^2$; $V_e = 14.295 \text{ km/sec}$; $\gamma_e = -11^\circ$).

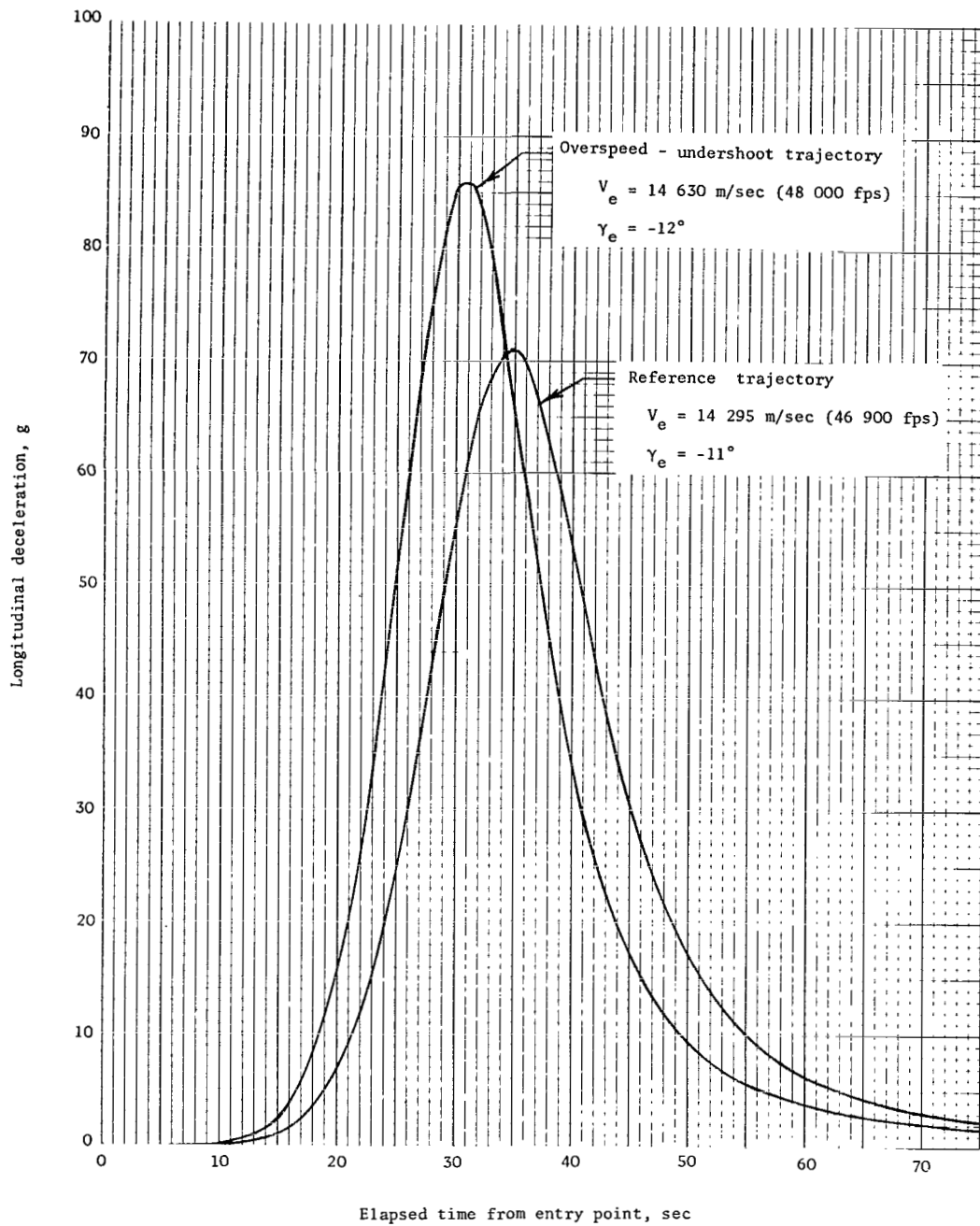


Figure 3.- Variation of longitudinal deceleration with time during entry.

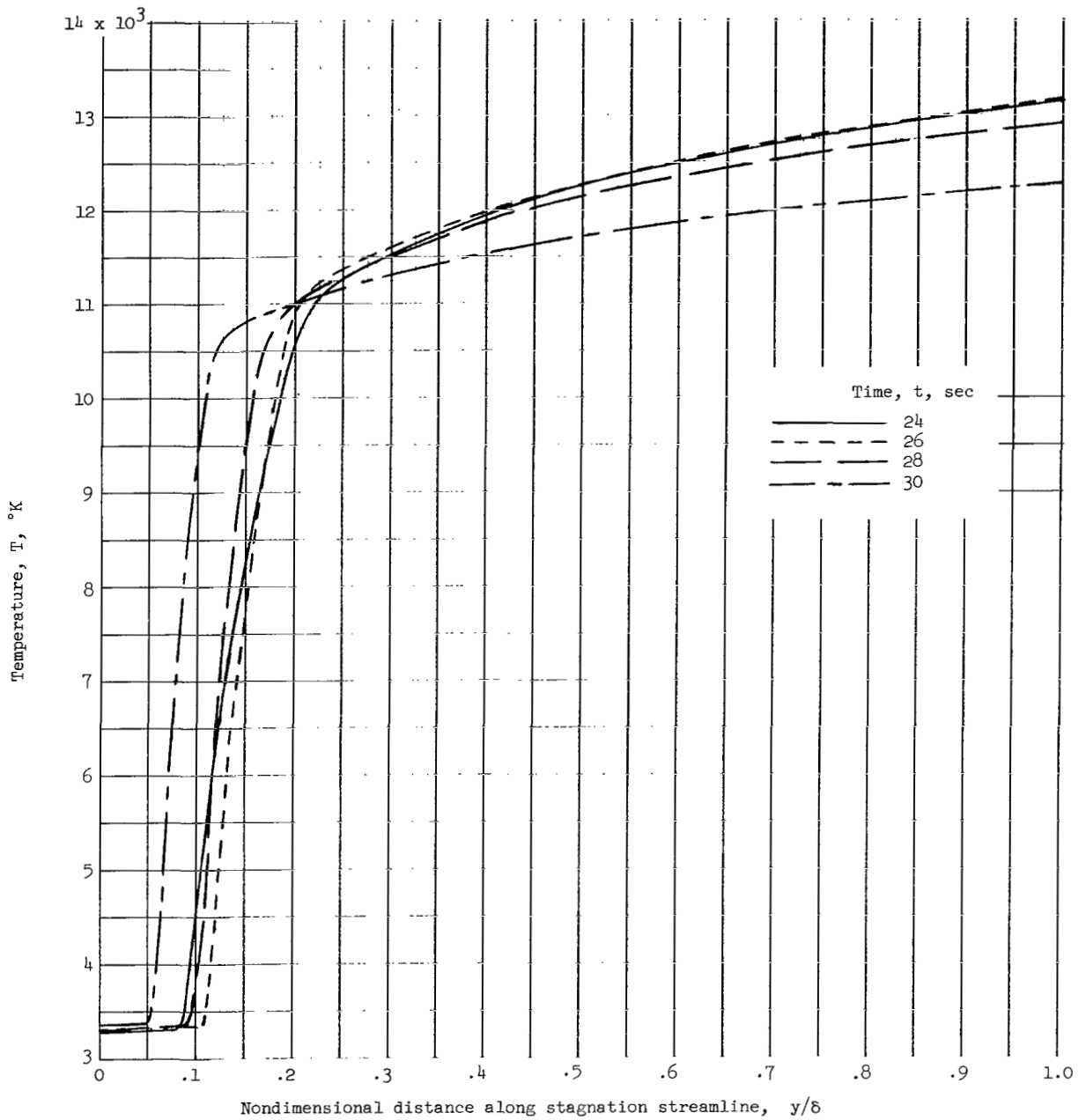


Figure 4.- Stagnation streamline temperature profiles for various times during reentry.

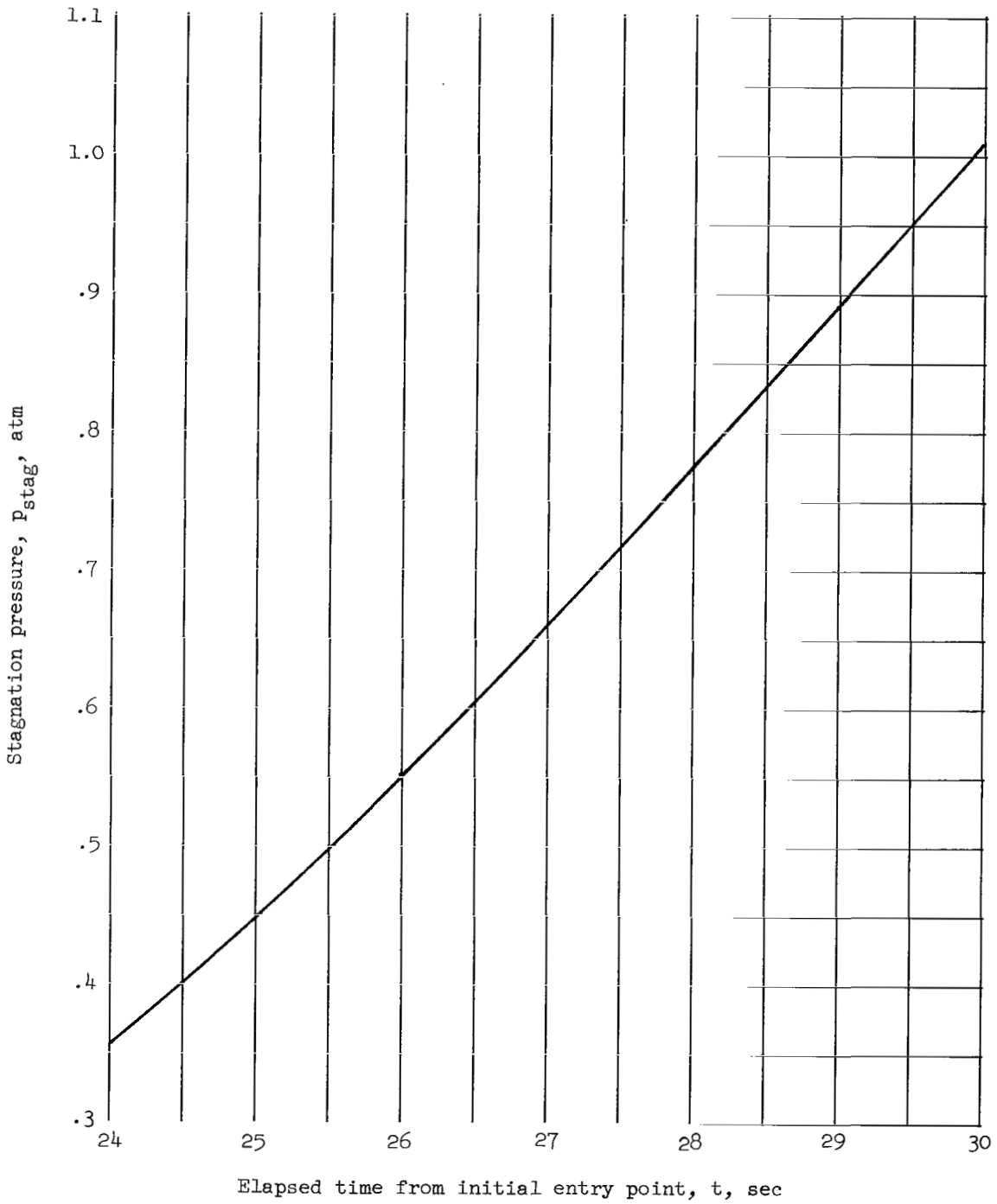


Figure 5.- Variation of stagnation-point pressure with time during reentry.

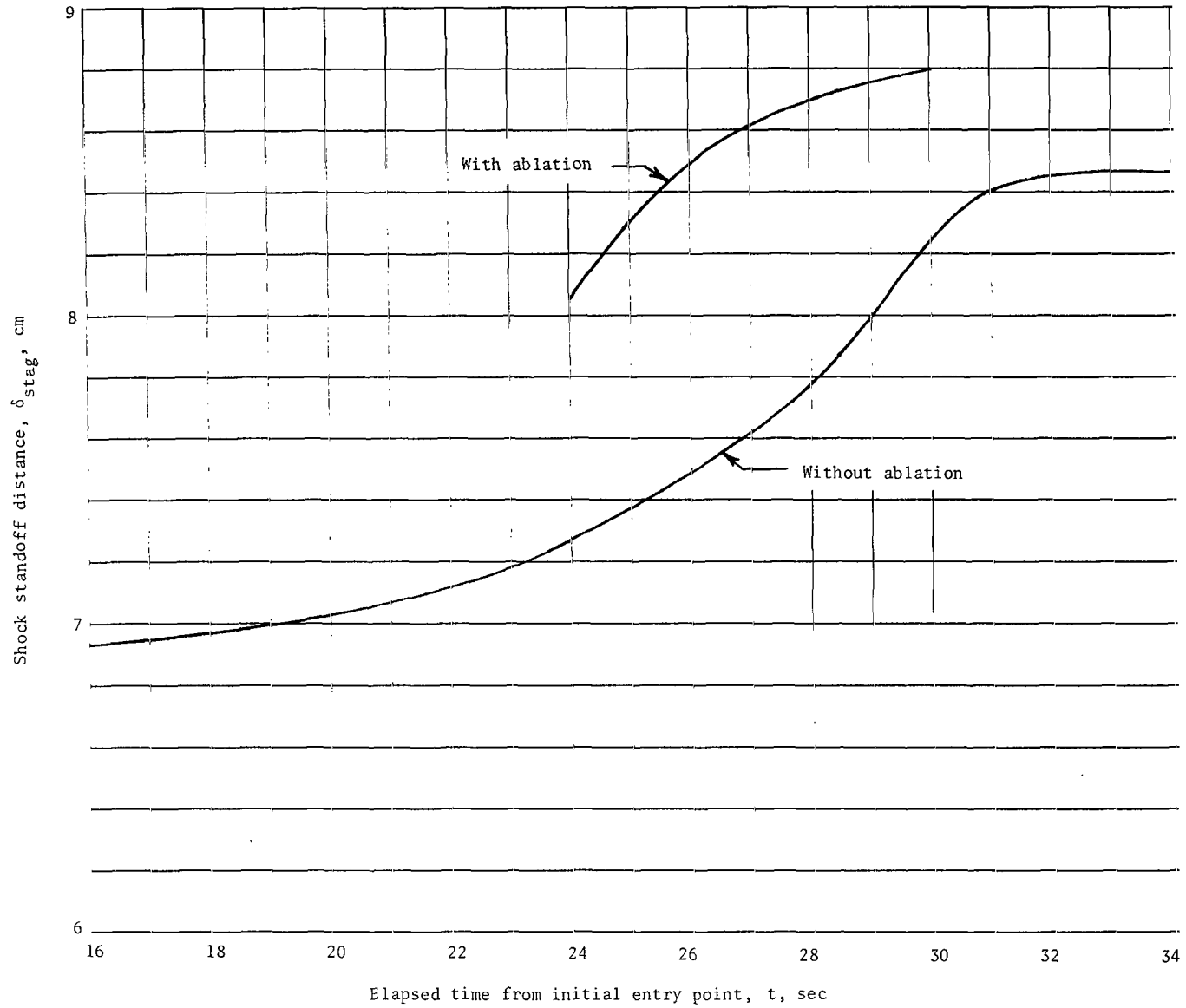


Figure 6.- Variation of shock standoff distance at stagnation streamline.

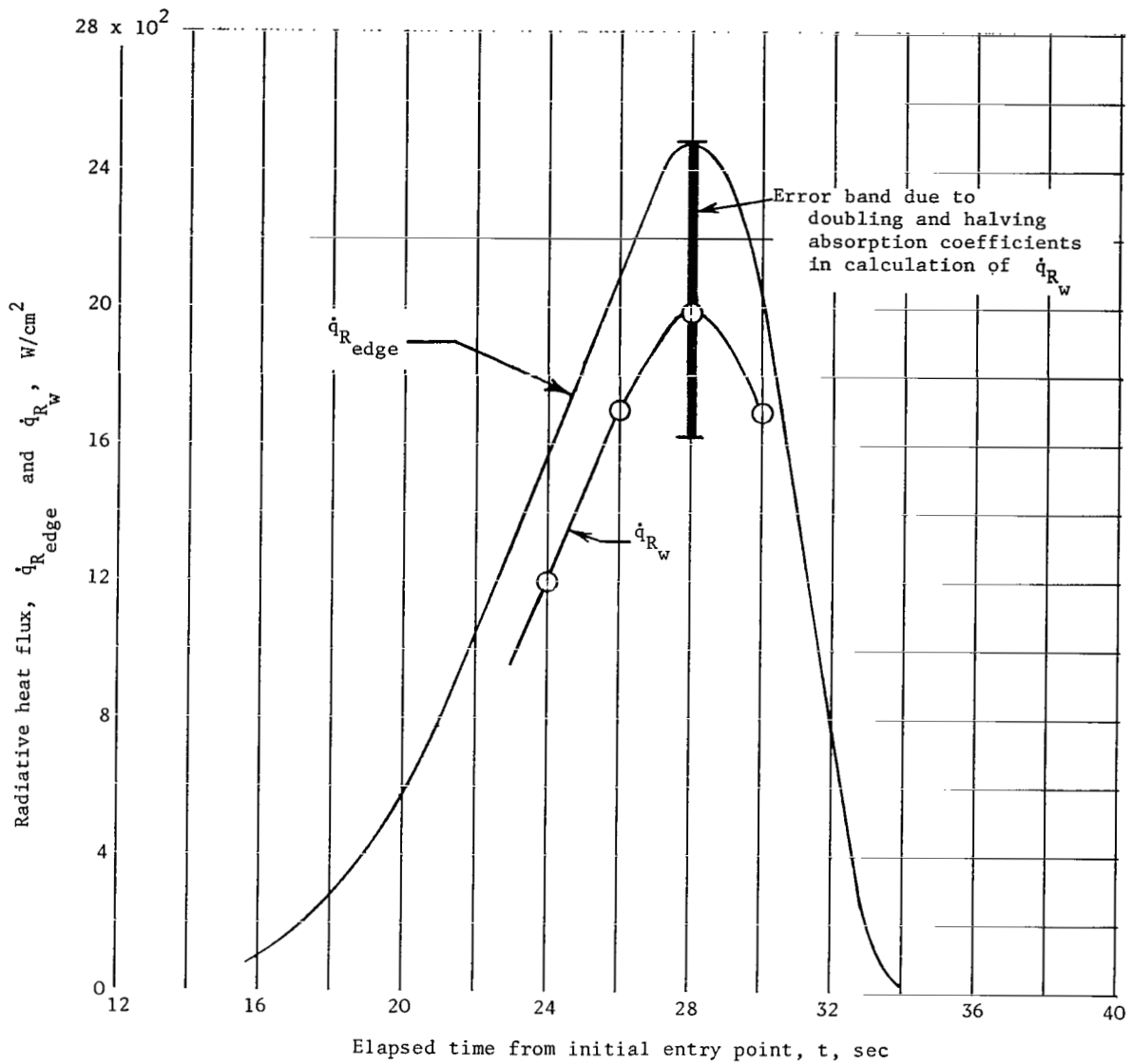


Figure 7.- Comparison of radiative heating rates at wall and at edge of boundary layer on stagnation streamline.

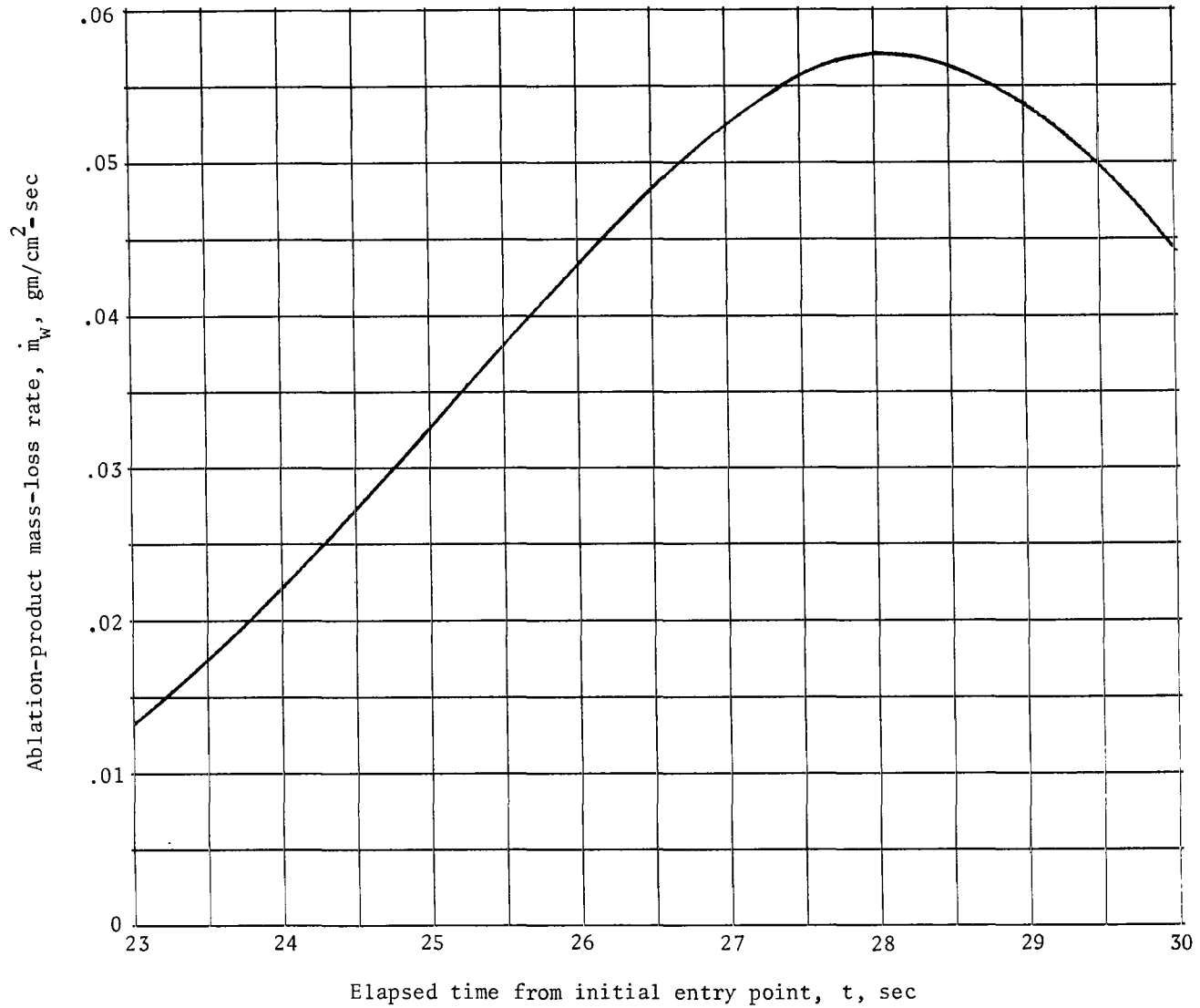


Figure 8.- Variation of heat-shield mass-loss rate at stagnation point.

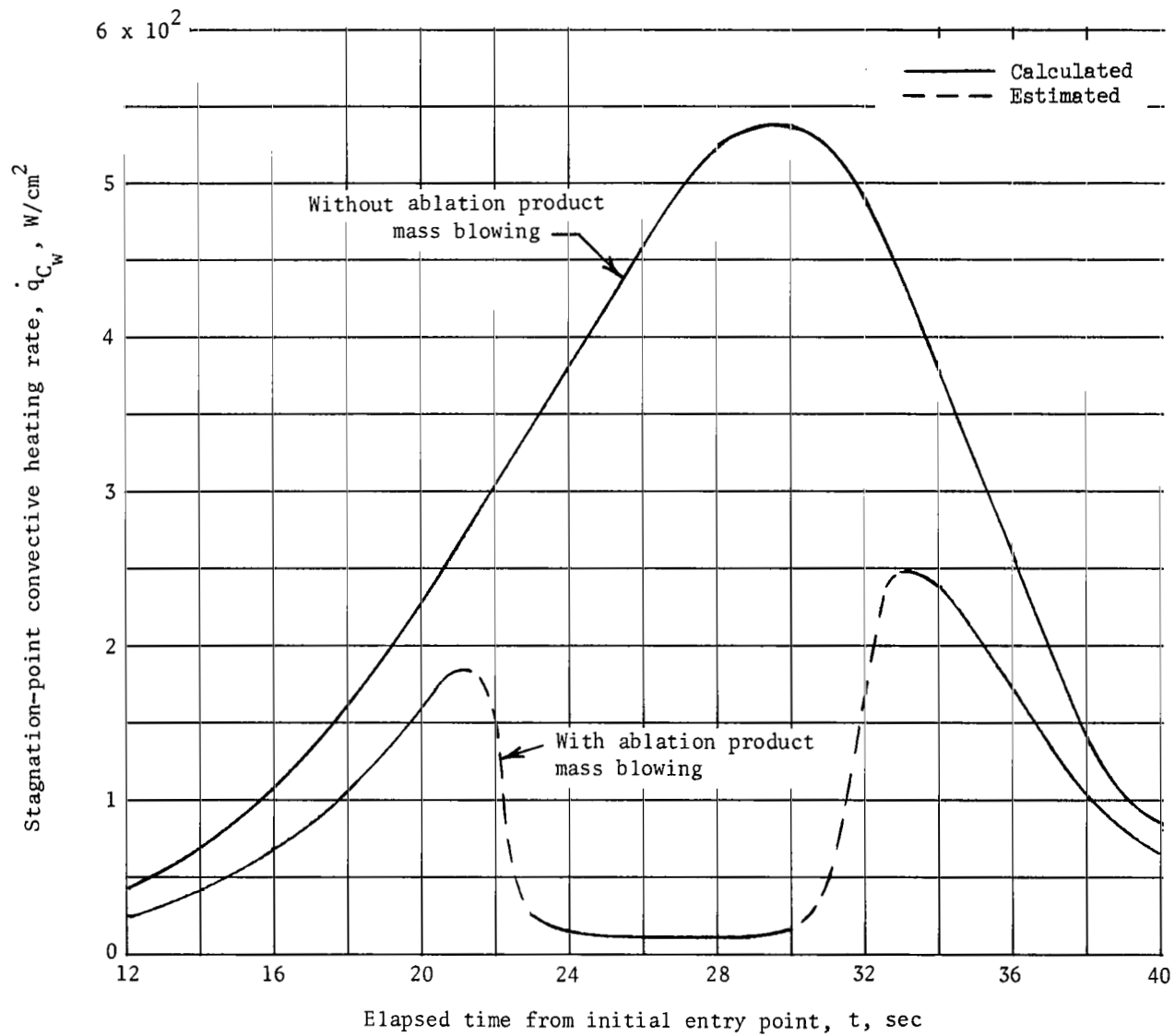
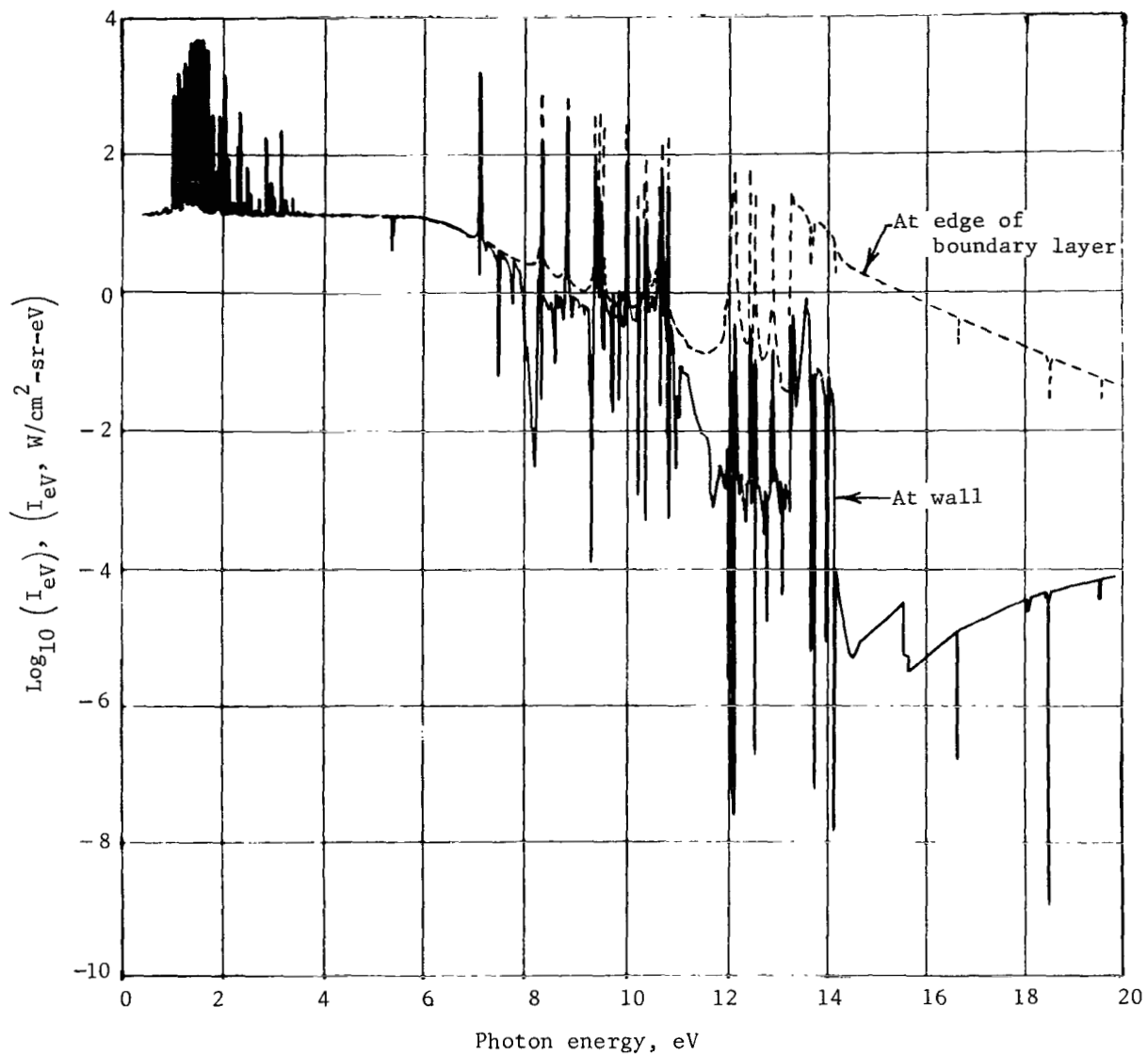
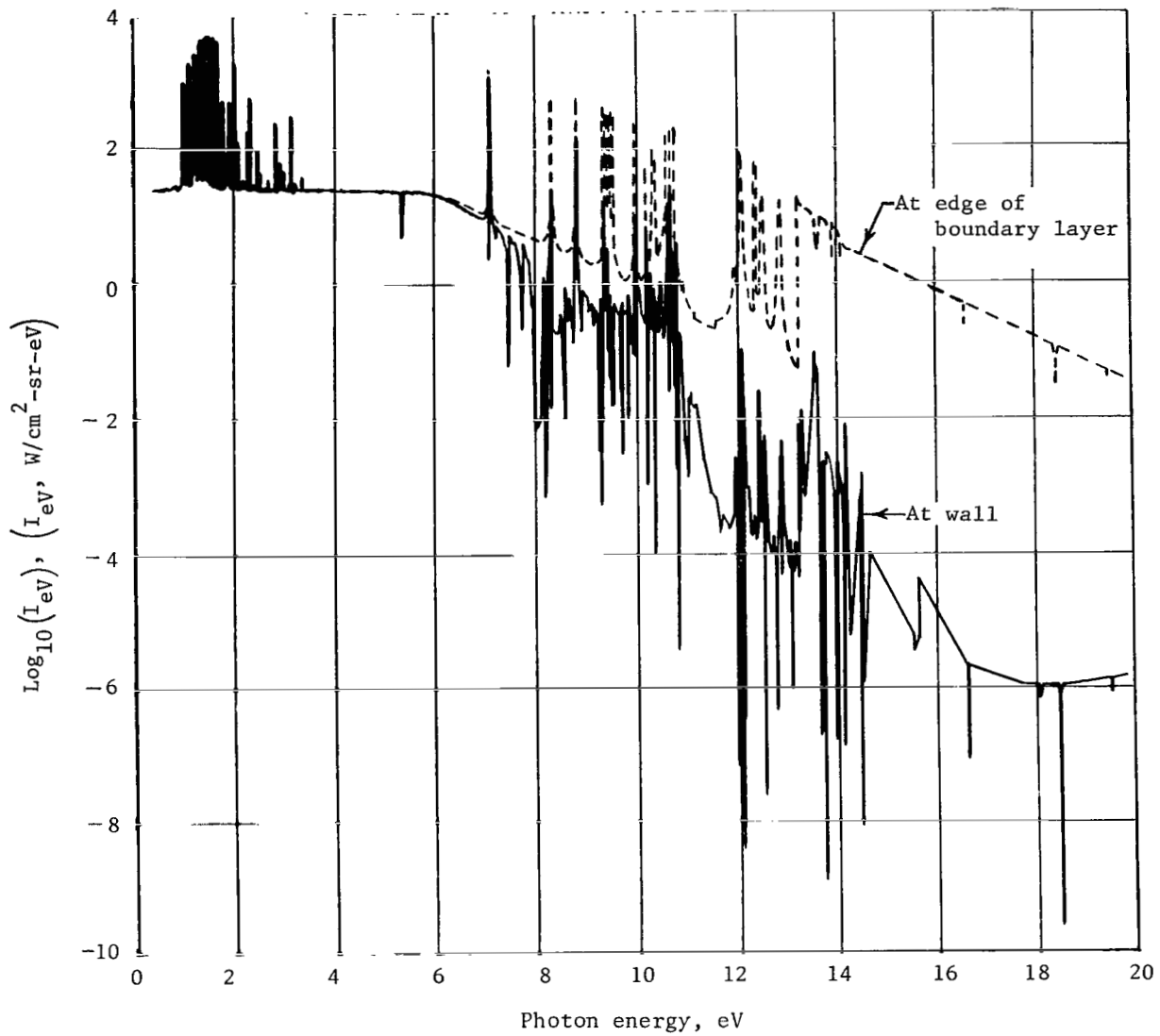


Figure 9.- Effect of mass blowing of ablation products on stagnation-point convective heating rates.



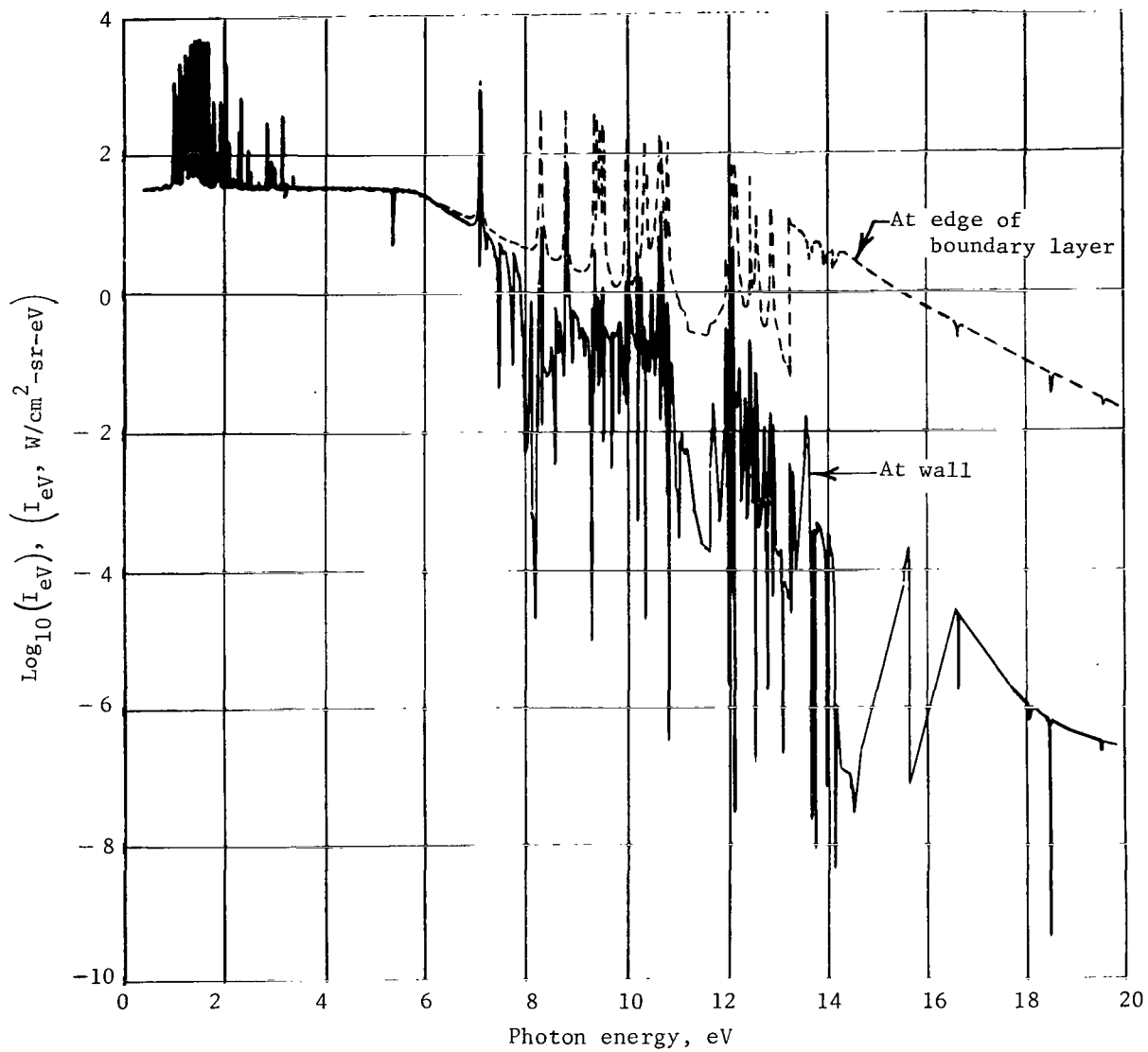
(a) $t = 24$ sec.

Figure 10.- Stagnation-point radiation intensity spectra for selected times during reentry.



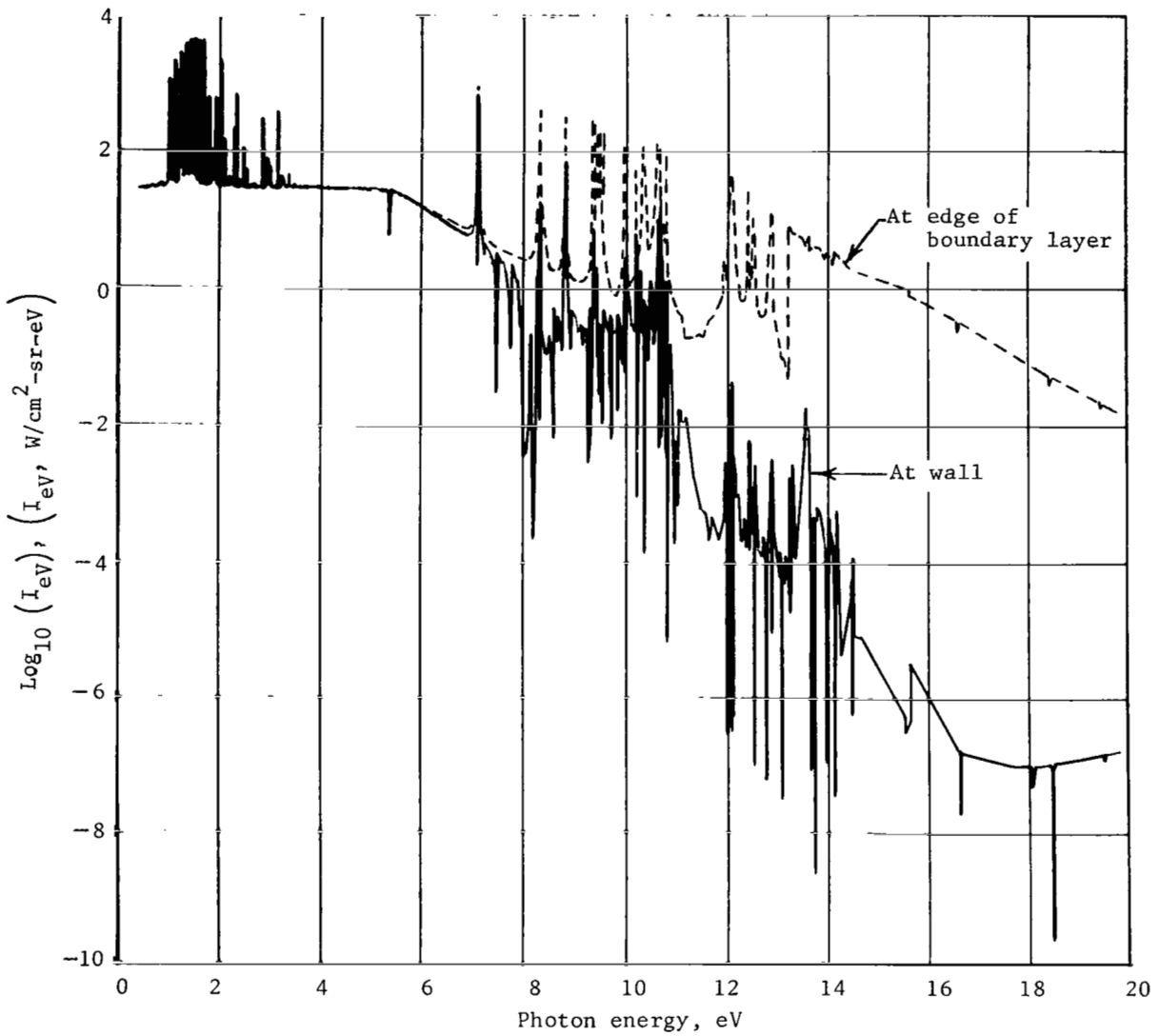
(b) $t = 26$ sec.

Figure 10.- Continued.



(c) $t = 28$ sec.

Figure 10.- Continued.



(d) $t = 30 \text{ sec.}$

Figure 10.- Concluded.

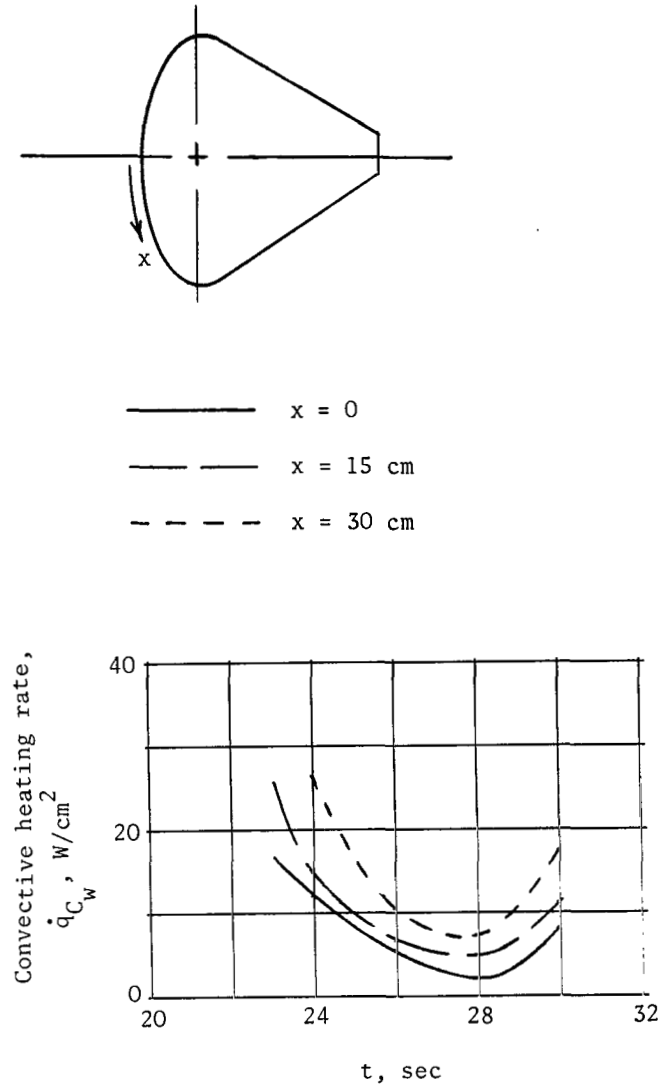
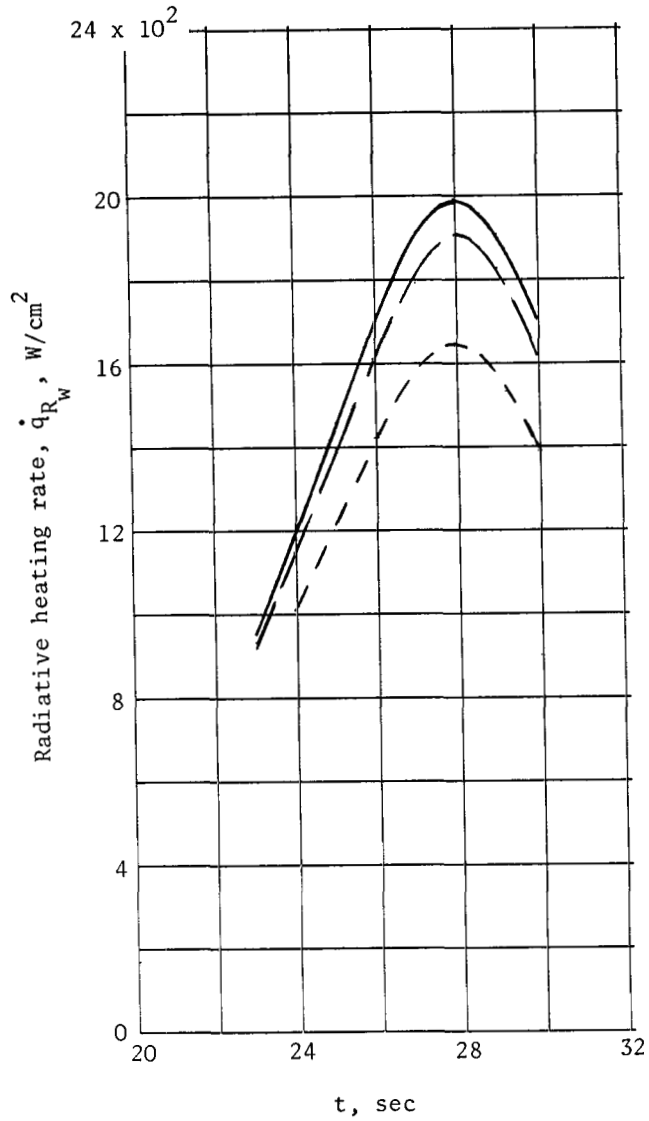


Figure 11.- Comparison of heating rates at three different radial locations on forebody heat shield.

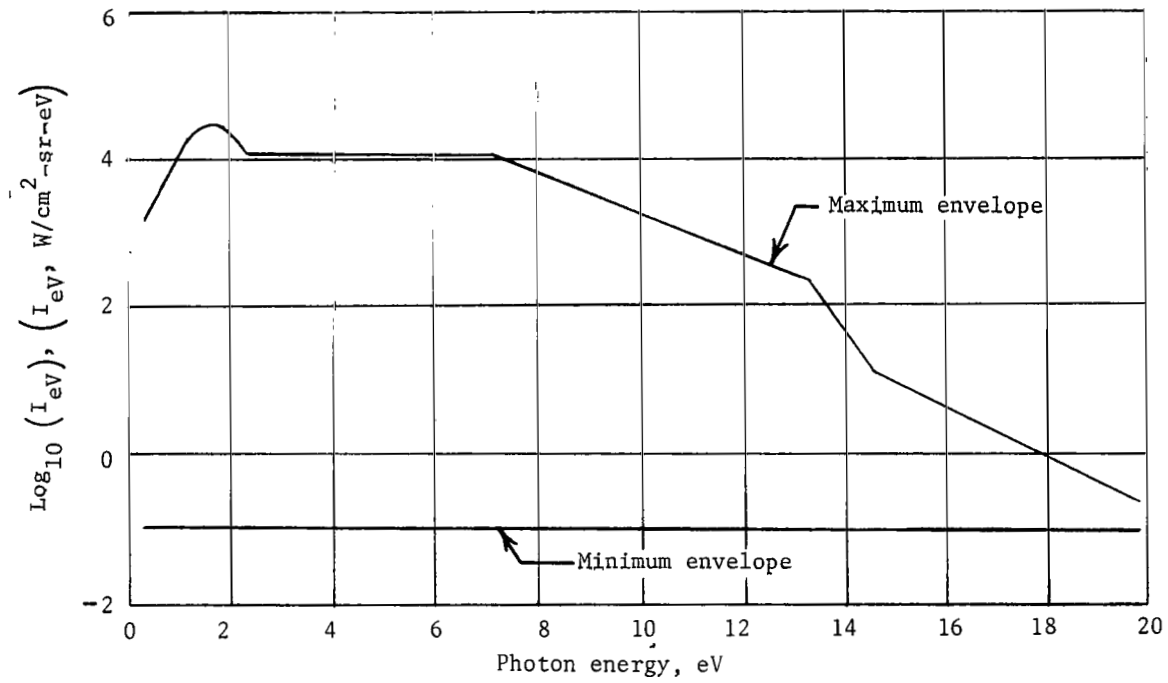


Figure 12.- Estimated maximum and minimum radiation intensity measurement requirements.

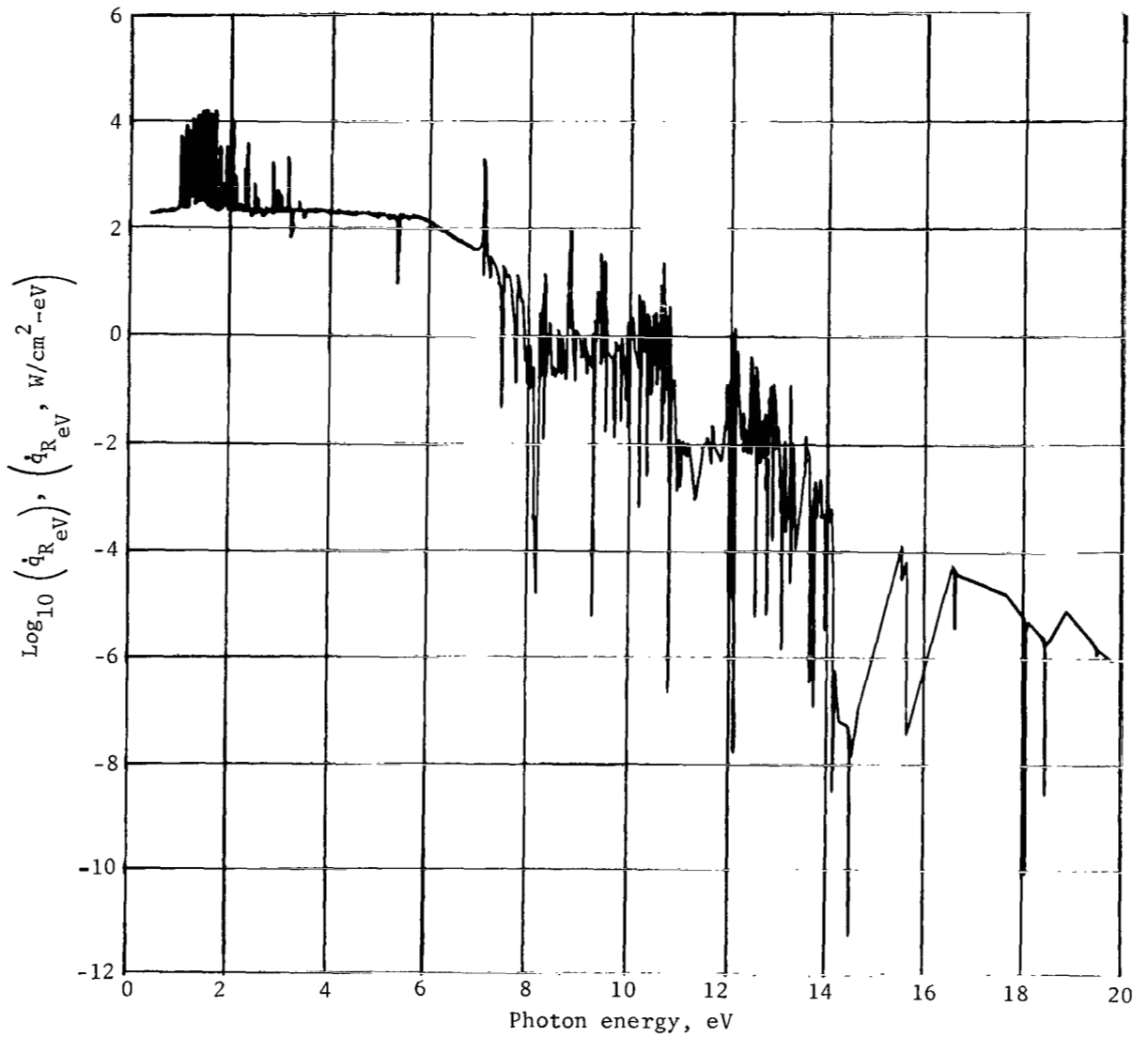


Figure 13.- Stagnation-point spectral radiative heat flux for time of peak heating ($t = 28$ sec).

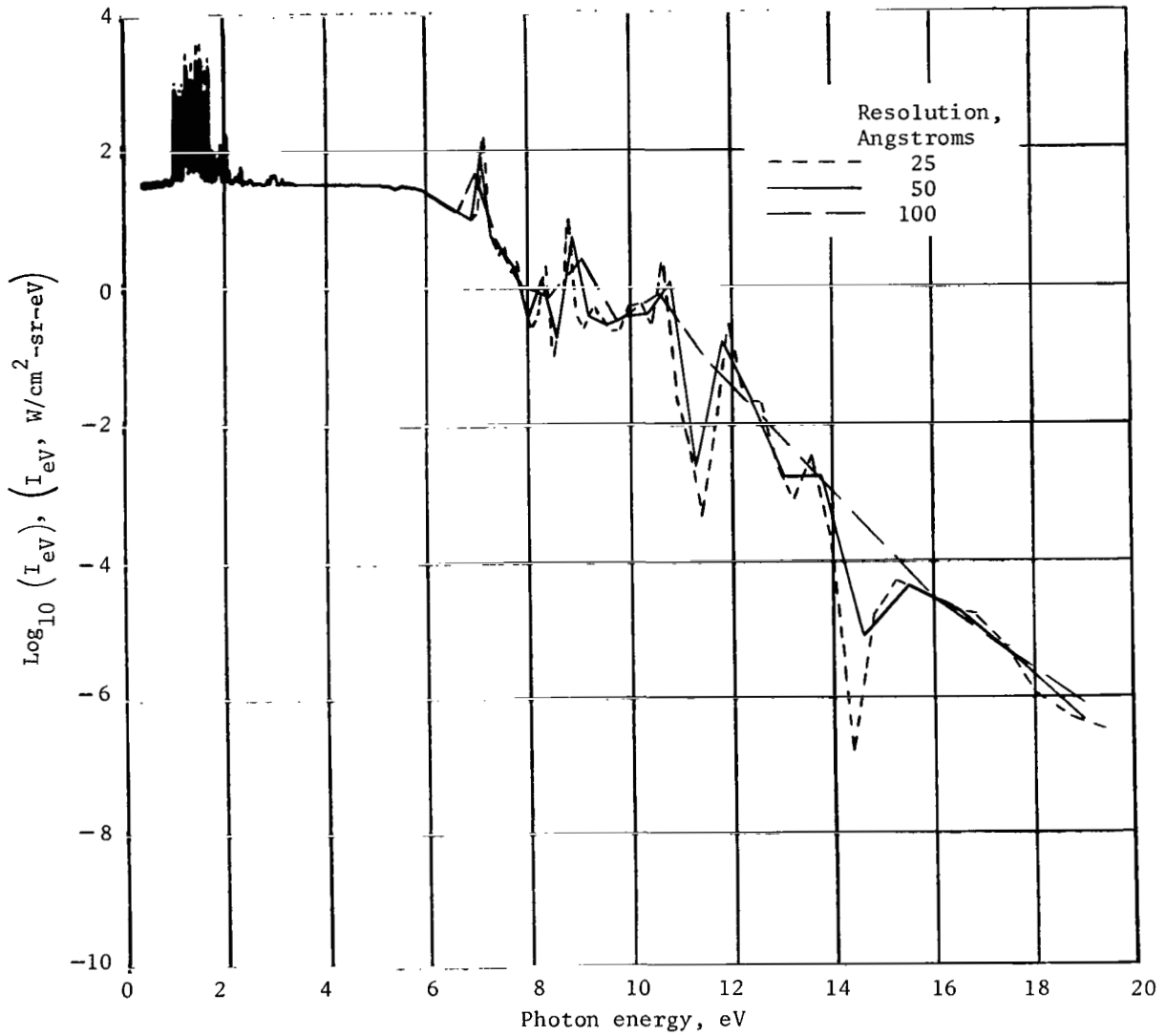


Figure 14.- Effect of radiometer resolution on appearance of measured radiation intensity spectrum. Stagnation point; $t = 28$ sec.

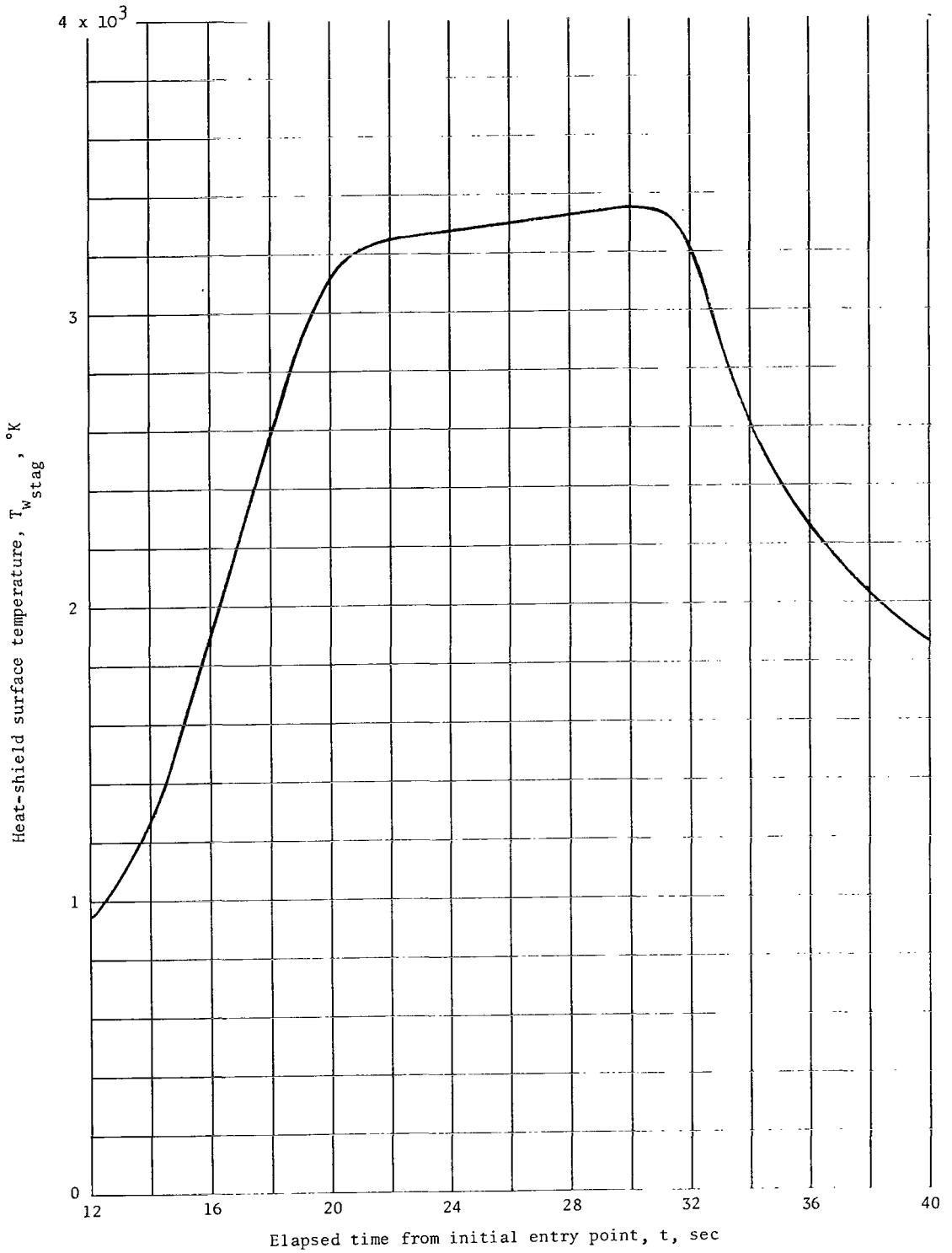


Figure 15.- Heat-shield surface-temperature history of stagnation point.

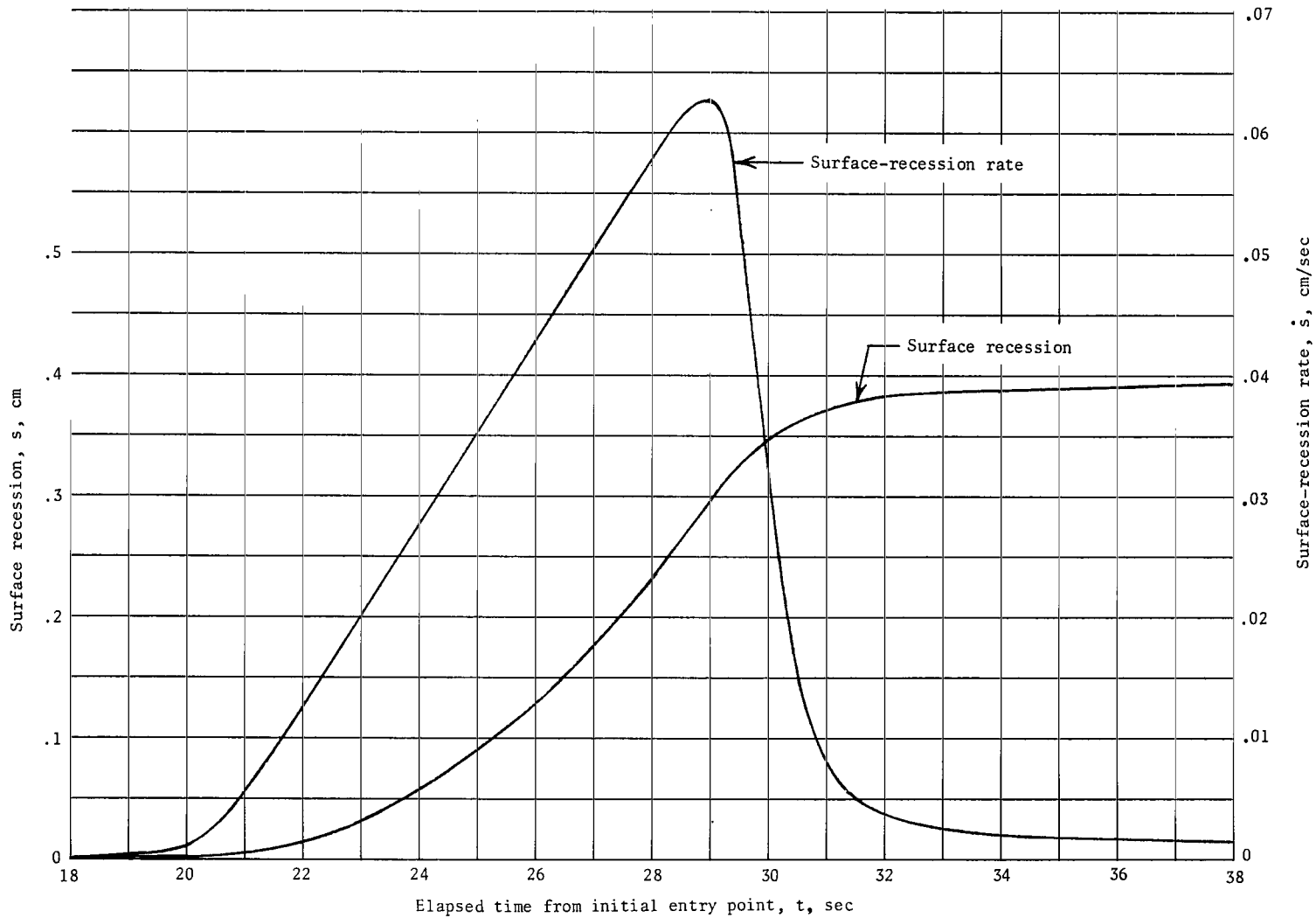


Figure 16.- Variation of heat-shield surface recession and surface-recession rate at stagnation point. 1.2-gm/cm³ phenolic-nylon heat shield.

NATIONAL AERONAUTICS AND SPACE ADMINISTRATION
WASHINGTON, D. C. 20546

OFFICIAL BUSINESS
PENALTY FOR PRIVATE USE \$300

FIRST CLASS MAIL



POSTAGE AND FEES PAID
NATIONAL AERONAUTICS AND
SPACE ADMINISTRATION

03U 001 39 51 3DS 71166 00903
AIR FORCE WEAPONS LABORATORY /WLOL/
KIRTLAND AFB, NEW MEXICO 87117

ATT E. LOU BOWMAN, CHIEF, TECH. LIBRARY

POSTMASTER: If Undeliverable (Section 1505
Postal Manual) Do Not Return

"The aeronautical and space activities of the United States shall be conducted so as to contribute . . . to the expansion of human knowledge of phenomena in the atmosphere and space. The Administration shall provide for the widest practicable and appropriate dissemination of information concerning its activities and the results thereof."

— NATIONAL AERONAUTICS AND SPACE ACT OF 1958

NASA SCIENTIFIC AND TECHNICAL PUBLICATIONS

TECHNICAL REPORTS: Scientific and technical information considered important, complete, and a lasting contribution to existing knowledge.

TECHNICAL NOTES: Information less broad in scope but nevertheless of importance as a contribution to existing knowledge.

TECHNICAL MEMORANDUMS: Information receiving limited distribution because of preliminary data, security classification, or other reasons.

CONTRACTOR REPORTS: Scientific and technical information generated under a NASA contract or grant and considered an important contribution to existing knowledge.

TECHNICAL TRANSLATIONS: Information published in a foreign language considered to merit NASA distribution in English.

SPECIAL PUBLICATIONS: Information derived from or of value to NASA activities. Publications include conference proceedings, monographs, data compilations, handbooks, sourcebooks, and special bibliographies.

TECHNOLOGY UTILIZATION PUBLICATIONS: Information on technology used by NASA that may be of particular interest in commercial and other non-aerospace applications. Publications include Tech Briefs, Technology Utilization Reports and Technology Surveys.

Details on the availability of these publications may be obtained from:

SCIENTIFIC AND TECHNICAL INFORMATION OFFICE

NATIONAL AERONAUTICS AND SPACE ADMINISTRATION

Washington, D.C. 20546